

Spectral and polarization properties of photonic cholesteric liquid crystals with defects of structure

Maxim V. Pyatnov

Institute of Engineering Physics and Radio Electronics
Siberian Federal University
Krasnoyarsk, Russia 2017

Maxim V. Pyatnov, 2017

ISBN

Published by Siberian Federal University, Krasnoyarsk, Russia

TABLE OF CONTENTS

TABLE OF FIGURES	4
ABSTRACT	7
LIST OF ARTICLES PUBLISHED	10
ACKNOWLEDGEMENTS	11
1. Theoretical background	12
1.1 Cholesteric liquid crystal as a one-dimensional photonic crystal	12
1.2 Technique for calculating the spectral properties of complex one-dimensional anisotropic structures	15
2. Photonic defect modes in cholesteric liquid crystal with a resonant nanocomposite layer	22
2.1. Optics of CLCs with defect of structure.....	22
2.2. Isotropic nanocomposite defect layer.....	24
2.3. Transmission spectra of CLC with isotropic resonance defective nanocomposite layer.....	28
2.4. Controlling of transmission spectrum of CLC with combined defect layer.....	34
3. Optical localized states in structures containing cholesteric liquid crystal ... 39	
3.1. Surface electromagnetic waves	39
3.2. Localized optical states in a ‘photonic cholesteric liquid crystal – phase plate – metal’ structure.....	41
3.2.1. Surface localized modes.....	41
3.2.2. Transmission anisotropy.....	46
3.2.3. Controlling the transmission spectrum of the structure.....	49
3.3. Localized optical states in a structure formed by two oppositely handed cholesteric liquid crystal layers and a metal.....	53
3.4. Localized optical states in a liquid-crystal structure adjacent to a metal....	60
SUMMARY	64
REFERENCES	66

LIST OF FIGURES

Figure 1.1. 1D, 2D, 3D photonic crystals.....	13
Figure 1.2. Schematic of a cholesteric liquid crystal.....	14
Figure 2.1. Schematic of CLC with a combination of defects.....	24
Figure 2.2. Imaginary ε''_{mix} (dashed curve) and real ε'_{mix} (solid curve) parts of the effective permittivity of ε_{mix} versus wavelength. The filling factor $f = 0.02$ (a), 0.1 (b).....	26
Figure 2.3. Transmission spectrum for right- (solid curve) and left-handed (dashed curve) polarizations for $\alpha = 0, f = 0$	28
Figure 2.4. (a) Transmission, (b) reflection, and (c) absorption spectra for waves with the right-handed (solid line) and left-handed (dashed line) circular polarizations, $\theta = 0^\circ$. The filling factor is $f = 0.02$	30
Figure 2.5. Transmission spectra of the structure for various α : (a) $\alpha > 0$, (b) $\alpha < 0$. Bold curves refer to the right-handed and thin curves to left-handed circular polarizations of light $f = 0.02$	31
Figure 2.6. Distribution of the squared electric field modulus in defect modes with $\lambda = 388.2$ nm (Option 3 in Figure 2.5a). (a) Wave with right-handed circular polarization, (b) Wave with left-handed circular polarization. $f = 0.02$	32
Figure 2.7. Transmission spectrum for various helix pitches. (a) $p = 305$ nm, (b) $p = 320$ nm. Solid and dashed curves refer to the right-handed and left-handed circular polarizations of light, respectively. $f = 0.02, \alpha = -30^\circ$	35
Figure 2.8. Transmission coefficient for a system of two cholesterics with a defect (solid curve) and for each of the cholesterics (dashed curve) with the pitch on the left of the defect $p_1 = 275$ nm (cyan dotted curve) and $p_2 = 290$ nm (red dotted curve). The remaining parameters are the same as in Figure 2.3.....	36

Figure 2.9. Maximum squared modulus of the electric field of the defect mode as a function of the pitch p_2 . The remaining parameters are the same as in Figure 2.3.....	37
Figure 2.10. Transmission spectra for various p_2 : Solid curve $p_2 = 275$ nm, dashed curve $p_2 = 290$ nm, dash-and-dotted curve $p_2 = 305$ nm, $\alpha = -30^\circ$	38
Figure 2.11. Maximum of the squared electric field modulus of the long-wavelength defect mode as a function of the pitch p_2 , $\alpha = -30^\circ$. Bold curves refer to the right-handed and thin curves to the left-handed circular polarizations of light, $f = 0.01$	38
Figure 3.1. Schematic of the ‘CLC– phase plate – metal’ structure.....	41
Figure 3.2. Transmission versus wavelength with light incidence normal to CLC (dashed line), to the silver film (dash-dotted line) and to the ‘CLC– phase plate – metal’ structure (solid line).....	42
Figure 3.3. Distribution of the squared modulus of the electric field intensity $ E(z) ^2$ in the ‘CLC– phase plate – metal’ structure for $\lambda = 586$ nm. Field is normalized to the input field equal to unity.....	43
Figure 3.4. Localization of light for right-hand (R) and left-hand (L) polarizations in the structures consisting of (a, b) the CLC and metal layers and (c, d) the CLC layer, phase plate, and metal layer.....	45
Figure 3.5. Transmission spectrum of the structure for incident waves with (a) the right-hand and (b) left-hand circular polarization. Solid line corresponds to the incidence on the CLC and dashed line, to the incidence on the metal.....	47
Figure 3.6. Light polarization dynamics at the incidence (a, b) on the CLC and (c, d) on the metal. R and L are the right- and left-hand circular polarization and “linear” is the linear polarization.....	48

Figure 3.7. Transmission spectrum associated with different polarizations of light tunneling through the localized mode.....	49
Figure 3.8. (a) Transmittances corresponding to the localized state at different φ for the light falling on the CLC (solid line) and on the metal (dashed line). (b) Electric field intensity at the OTS frequency at different φ for the light falling on the CLC (solid line) and on the metal (dashed line).....	51
Figure 3.9. Transmission spectrum of the structure versus cholesteric helix pitch.....	52
Figure 3.10. The maximum local intensity of the electric field (in units of the incident field intensity) at the localized state frequency, depending on the CLC helix pitch.....	52
Figure 3.11. Schematic of the structure consisting of two oppositely handed CLCs and a metal layer.....	53
Figure 3.12. Transmission spectrum of the structure for circular polarizations.....	54
Figure 3.13. Localization of light with the right circular polarization at $\lambda=591$ nm.....	55
Figure 3.14. The dependence of wavelength for maximum transmission for right circular polarization vs angle α	56
Figure 3.15. Electric field intensity for maximal localization wavelength vs metal thickness at the light incidence onto the CLC and the metal.....	57
Figure 3.16. The dependence of transmission spectrum for the right-handed circular polarization on period number of the two CLCs; $\alpha = 0$	58
Figure 3.17. Schematic of the experimental structure.....	59
Figure 3.18. Schematic of the investigated structure.....	60
Figure 3.19 Transmission spectrum of the structure for circularly polarized incident light.....	61

Figure 3.20.Electric-field-intensity distribution for right-hand circular polarization of the incident light at a wavelength of 603.5 nm.....62

Figure 3.21. Dependence of the transmission spectrum for right-hand circular polarization on number of periods d between the defect and metal.....63

ABSTRACT

Photonic crystals (PCs) attract much attention, first of all, due to the prospects of their application in optoelectronics and photonics. The specific feature of these materials is the periodic variation of their permittivity in one, two, or three dimensions with a spatial periodicity comparable with the light wavelength. In the band gap of a PC with a lattice defect, i.e., with a broken periodicity, the transmission bands with controllable position and transmittance are formed. In this case, light is localized in the defect region, which leads to an increase in the light wave intensity inside the defect layer.

The possibility of manipulating by the photonic band structure using external factors is extremely important for many applications. It is well-known that liquid crystals exhibit the high sensitivity to external fields and strong anisotropy of the permittivity. An interesting type of liquid crystals is cholesteric liquid crystals (CLCs), which exhibit all the properties of PCs and form a special class of chiral PCs.

New opportunities for governing light occur in one-dimensional PCs with the nanostructured metal-dielectric defect layers. The occurrence of the effective permittivity resonance was predicted for a nanocomposite consisting of metal nanoparticles dispersed in a transparent matrix, whereas the optical characteristics of the initial materials have no resonance features. The position of the resonance localized in the visible spectral range depends on permittivity of the initial materials and concentration and shape of nanoparticles.

At present, the surface properties of PCs evoke great interest. In particular, a special type of localized electromagnetic states excited at the normal incidence of light called the optical Tamm states (OTSs) has been intensively investigated. This phenomenon is used in various devices, including sensors, solar cells, and lasers. Therefore, the experimental and theoretical study of the OTSs in tunable PC structures based on CLCs is very promising.

The aim of this study was to theoretically investigate the spectral and polarization properties of PC structures based on CLCs.

In the course of this work, the following problems were solved:

(i) Study of photonic defect modes in a CLC combining an isotropic nanocomposite layer with the resonant dispersion and twist defect.

(ii) Study of the localized optical states in the structure “CLC – quarter-wave plate – metal”.

(iii) Study of the localized optical states in a structure formed by two oppositely twisted CLC layers and a metal.

(iv) Study of the localized optical states in a system consisting of the defect-containing CLC and metal.

The obtained results were reported at several international and domestic scientific conferences.

The importance of the conducted fundamental investigations of spectral and polarization properties of PC CLCs with inclusions of resonant nanocomposites and anisotropic materials is determined by the significantly broadened possibility of controlling the parameters of the photon energy spectrum, and transmission, reflection, and absorption spectra of CLCs and the high potential of these materials for application in new optoelectronic and photonic devices.

Our study disclosed a number of important spectral and polarization features of the PC structures based on CLCs. New opportunities of controlling light with the high efficiency were demonstrated, which are characteristic of only the chiral media.

Defect modes in a CLC combining a nanocomposite layer with the resonance dispersion and the twist defect were investigated. The spectral properties of such a structure are caused, first of all, by the resonance character of the nanocomposite effective permittivity and its significant dependence on the filling factor. The phase shift of a cholesteric helix is a nontrivial control technique, which can only be implemented in chiral PCs. The transmission

spectrum of the investigated structure can be effectively tuned by changing the direction and value of the twist defect.

We proposed three new models containing a CLC and a metallic layer, where the localized optical states are observed. The change in the wave polarization upon reflection from the metal and the specific polarization properties of CLCs require a phase-changing element to be embedded in the structure. Such an element can be the anisotropic quarter-wave layer, oppositely handed CLC, or defect CLC. The mechanism of light localization in the investigated systems was explained in detail. It was demonstrated that the transmission spectra of light propagating in the forward and backward directions for a model containing the quarter-wave element are different; i.e., we observe the transmission anisotropy. Therefore, the investigated structure can be used as a polarization optical diode based on the surface photonic modes.

The possibility of effective control of the transmission spectrum was demonstrated for all the investigated systems. Manipulation by the transmission peak position via changing the CLC helix pitch using external fields and other parameters characteristic of specific systems were investigated.

LIST OF ARTICLES PUBLISHED

1. Specific Features of the Spectral Properties of a Cholesteric Liquid Crystal with a Resonance Defective Nanocomposite Layer / S. Ya. Vetrov, M. V. Pyatnov, I. V. Timofeev // *Physics of the Solid State*. – 2013. – V. 55. – P. 1697–1702.
2. Photonic defect modes in a cholesteric liquid crystal with a resonant nanocomposite layer and a twist defect / S. Ya. Vetrov, M. V. Pyatnov, I. V. Timofeev // *Physical Review E*. – 2014. – V. 90. – P. 032505.
3. Surface modes in “photonic cholesteric liquid crystal–phase plate–metal” structure / S. Ya. Vetrov, M. V. Pyatnov, I. V. Timofeev // *Optics Letters*. – 2014. – V. 39. – P. 2743–2746.
4. Spectral and polarization properties of a ‘cholesteric liquid crystal—phase plate—metal’ structure / S. Ya. Vetrov, M. V. Pyatnov, I. V. Timofeev // *Journal of Optics*. – 2016. – V. 18. – P. 015103.
5. Pyatnov, M. V. Localised optical states in a structure formed by two oppositely handed cholesteric liquid crystal layers and a metal / M. V. Pyatnov, S. Ya. Vetrov, I. V. Timofeev // *Liquid Crystals*. – 2017. – V. 44. – P. 674–678.
6. Pyatnov, M. V. Localized optical states in a liquid-crystal structure adjacent to a metal / M. V. Pyatnov, S. Ya. Vetrov, I. V. Timofeev // *Optics and Spectroscopy*. – 2017. – V. 123. – P. 183–190.

ACKNOWLEDGEMENTS

My deepest gratitude is to my supervisor, Prof. Stepan Ya. Vetrov, from whom I learnt how to be a good scientist.

I am grateful to my coauthor Dr. Ivan V. Timofeev who introduced me to the world of science.

1. Theoretical background

1.1. Cholesteric liquid crystal as a one-dimensional photonic crystal

Photonic crystals (PC) are 1D, 2D, or 3D materials with the permittivity periodically changing with a period comparable with the optical electromagnetic wavelength. Owing to the spatial periodicity, the electromagnetic waves in PCs have a band spectrum, similar to the case of the spatially periodic potential leading to the band spectrum of electrons [1–3].

If the optical phase difference between the beams reflected from the sequential lattice planes is equal to an integral number of wavelengths, we observe the constructive interference. This leads to the formation of photonic band gaps in the spectral composition of light waves transmitted through a crystal [4]. The occurrence of these waves indicates that the light in the specified spectral range cannot enter a PC or leave it in a specified direction.

Photonic crystals can be divided in three classes –1D, 2D, and 3D– in accordance with the character of the refractive index variation (Fig. 1.1). An important property of a PC is the high degree of localization of electromagnetic waves on lattice defects. In the PC with the lattice defect, i.e., the broken periodicity, additional energy levels arise, which correspond to the localized defect modes. The transmission bands arise in the photonic band gap, the positions of which can be tuned by changing the geometrical and structural parameters. In this case, light is localized in the defect region, which leads to an increase in the light wave intensity inside the defect layer.

A special class of self-assembling one-dimensional photonic crystals is formed by cholesteric liquid crystals (CLCs), which have unique properties: a wide passband, strong nonlinearity, and high sensitivity to external fields [5,6]. The molecules in the cholesteric are ordered in such a way that, despite the absence of order in the arrangement of their centers of gravity, there is a long-range order in their orientation.

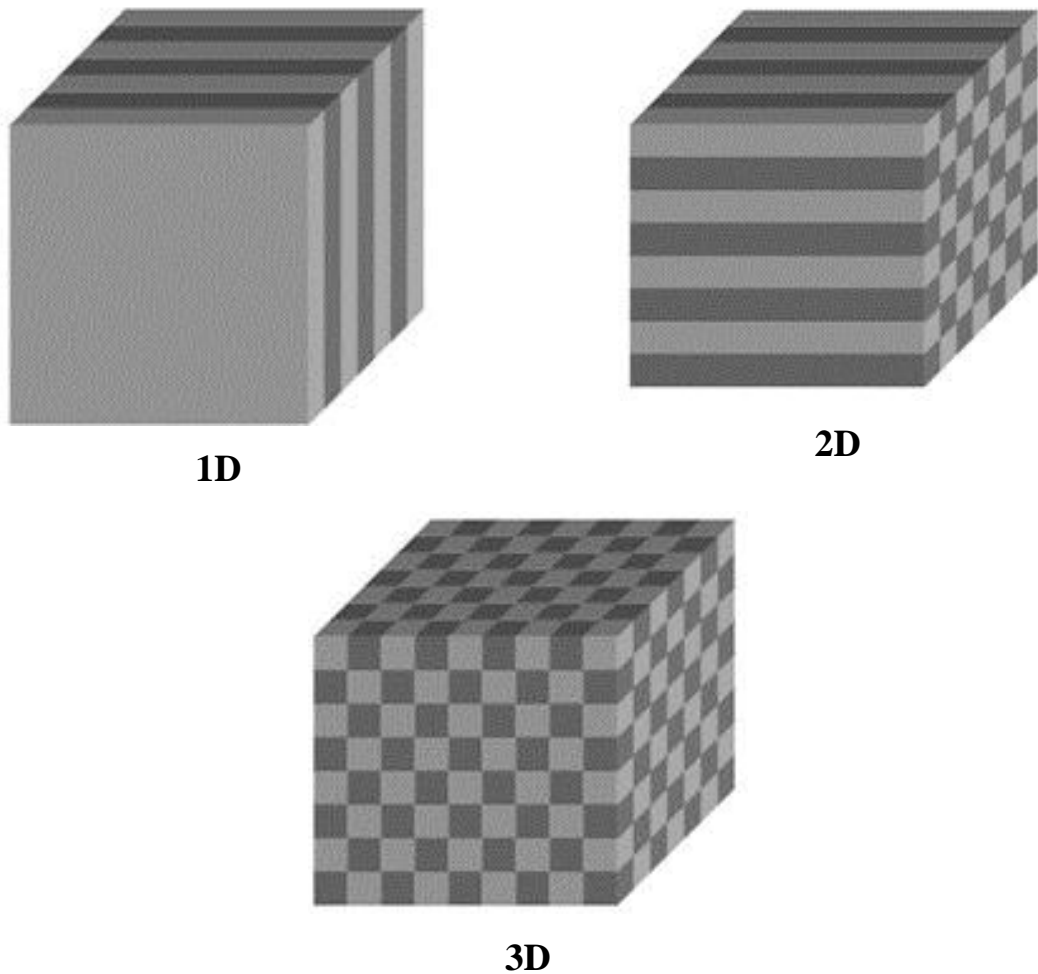


Figure 1.1. 1D, 2D, 3D photonic crystals.

CLCs are formed by elongated molecules arranged in helical structures. On average, these molecules are oriented similarly in the plane perpendicular to the helix axis. Their orientation direction is characterized by a director. The director continuously rotates along the axis with the formation of a birefringent structure (Figure 1.2).

This spatial structure can have a period corresponding to a wavelength range from optical to infrared radiation. The main characteristic of the CLC is the helix pitch p at which the distance along the crystal axis at which the director rotates through an angle of 2π . At the normal incidence of light in the wavelength range of $pn_o < \lambda < pn_e$, where p is the helix pitch and n_o and n_e are the ordinary and extraordinary refractive indices, there is a CLC photonic band gap for the circular polarization with a handedness sign identical to that of the

helix. This circularly polarized radiation is reflected from the CLC with a reflectance depending on the layer thickness. There is the only selective reflection band in the spectrum for the light propagating along the helix axis. The radiation with the circular polarization different from the CLC helix handedness does not experience the diffraction reflection.

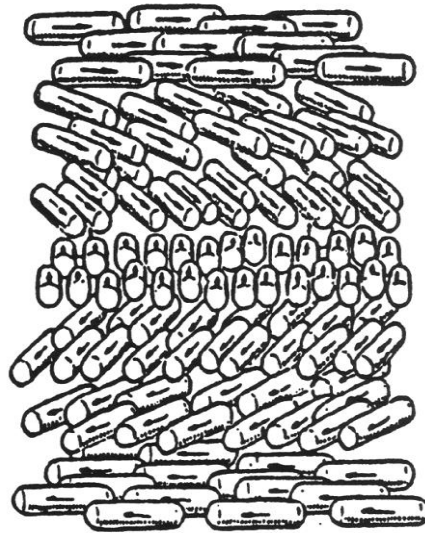


Figure 1.2. Schematic of a cholesteric liquid crystal.

In contrast to other types of one-dimensional PCs, for the CLC there exists the exact solution of the Maxwell equations at the normal incidence of light [7-10]. The eigensolutions are the superposition of two circularly polarized plane waves. These can be either two waves with the opposite circular polarizations propagating in one direction or two waves with the same circular polarization propagating in the opposite directions.

The advantage of CLCs is their tunability. The variations in temperature or external electric or magnetic fields and photoorientation effect can change the CLC structure, e.g., increase or decrease the cholesteric helix pitch and thereby change the band gap position. Another important feature of the CLCs is that it can have two or even three optically stable states. These remarkable properties allow the CLCs to be used in various optical devices.

1.2. Technique for calculating the spectral properties of complex one-dimensional anisotropic structures

The matrix forms of the Maxwell equations are most frequently used to describe the propagation of light through various optical media with plane-parallel boundaries. In terms of optics, CLCs are anisotropic birefringent media with permanent twisting. In the calculation of the spectral properties of such media, the inhomogeneous layer is divided into a sufficiently large number of sublayers, each being approximately homogeneous. At present, there exist several matrix methods for calculating the optical characteristics of different systems with arbitrary physical parameters.

Teitler and Henvis [11] and Berreman and Scheffer [12] developed a 4×4 matrix method for studying the reflection and transmission of the polarized light falling at a certain angle onto planar anisotropic layered structures. This method generalizes the Abelès 2×2 matrix method for isotropic layered media [13] based on the Jones matrix formalism [14]. The developed 4×4 matrix method is based on the general description proposed by Berreman [15]. This method was described in detail by Azzam and Bashara [16] and by Palto [17].

Let us consider the propagation of a plane polarized monochromatic wave in an anisotropic medium for an arbitrary orientation of the propagation direction relative to the optical axis of the medium. With the $e^{i\omega t}$ time dependence assumed the two Maxwell equations for the rotors take the form,

$$-\text{rot } \mathbf{E} = i\omega \mathbf{B}, \text{ rot } \mathbf{H} = i\omega \mathbf{D}, \quad (1.1)$$

where \mathbf{E} , \mathbf{H} , \mathbf{D} и \mathbf{B} are the electromagnetic-field vectors.

We assumed that plane monochromatic wave falls on anisotropic medium with plane-parallel boundaries. We choose a Cartesian coordinate system so that the z axis is parallel to the interface of the two media, and the x and y axes are

parallel to this boundary. Equations (1.1) can be combined into one matrix equation:

$$\mathbf{O}\mathbf{G}=i\omega/c\mathbf{C}, \quad (1.2)$$

\mathbf{O} is a 6×6 symmetric matrix operator which can be partitioned into four 3×3 submatrices to take the form

$$\mathbf{O} = \begin{bmatrix} 0 & \mathbf{rot} \\ -\mathbf{rot} & 0 \end{bmatrix}, \quad (1.3)$$

where 0 – 3×3 is zero matrix; \mathbf{rot} –rotor operator

$$\mathbf{rot} = \begin{bmatrix} 0 & -\partial/\partial z & \partial/\partial y \\ \partial/\partial z & 0 & -\partial/\partial x \\ -\partial/\partial y & \partial/\partial x & 0 \end{bmatrix}. \quad (1.4)$$

\mathbf{G} is a 6×1 column vector whose elements are the components of \mathbf{E} followed by those of \mathbf{H} , and \mathbf{C} is a 6×1 column vector whose elements are the components of \mathbf{D} followed by those of \mathbf{B} .

In the absence of nonlinear optical effects and spatial dispersion, the constitutive relation between \mathbf{C} and \mathbf{G} can be generally put as

$$\mathbf{C} = \mathbf{M}\mathbf{G}, \quad (1.5)$$

where the 6×6 matrix \mathbf{M} carries all the information about the anisotropic optical properties of the medium that supports the electromagnetic fields.

\mathbf{M} , to be called the optical matrix, can be conveniently partitioned as follows

$$\mathbf{M} = \begin{bmatrix} \varepsilon & \rho \\ \rho' & \mu \end{bmatrix}, \quad (1.6)$$

where $\varepsilon = (M_{kl})$ and $\mu = (M_{k+3l+3})$, $k, l = 1, 2, 3$ are the (dielectric) permittivity and (magnetic) permeability tensors;

$\rho = (M_{kl+3})$ and $\rho' = (M_{k+3l})$ are optical-rotation tensors.

Substitution of eq. (1.5) into eq. (1.2), yields $\mathbf{O}\mathbf{G} = i\omega/c\mathbf{M}\mathbf{G}$.

If in the above equation we replace \mathbf{G} by

$$\mathbf{G} = e^{i\omega t} \mathbf{\Gamma}, \quad (1.7)$$

where $\mathbf{\Gamma}$ is the spatial part of \mathbf{G} , it becomes

$$\mathbf{O}\mathbf{\Gamma} = i\omega/c\mathbf{M}\mathbf{\Gamma}. \quad (1.8)$$

Equation (1.8) is the spatial wave equation for frequency ω .

The particular problem under consideration involves the reflection and transmission of a monochromatic plane wave obliquely incident from an isotropic ambient medium ($z < 0$) onto an anisotropic planar structure ($z > 0$) stratified along the z -axis. The x -axis of the reference xyz Cartesian coordinate system is assumed to coincide with the line of intersection of the plane of incidence (the plane of the incident wave-vector and the z -axis) and the $z = 0$ interface (see fig. 4.38). From the symmetry of the problem, there is no variation in the y direction of any field component, so that

$$\partial/\partial y = 0 \quad (1.9)$$

For the tangential fields to match across the boundary $z = 0$, at all of its points at all time, all the waves that are excited by the incident plane wave must have the same spatial dependence in the x-direction as the incident wave. Therefore, if ζ denotes the x component of the wave-vector of the incident wave, all fields should vary in the x-direction as $ee^{-i\zeta x}$, hence

$$\partial/\partial x = -i\zeta \quad (1.10)$$

In terms of the refractive index N_0 of the ambient medium and the angle of incidence φ_0 , ζ is given by

$$\zeta = \omega/c N_0 \sin\varphi_0, \quad (1.11)$$

где c —is the free-space wavevelocity.

Use of equations (1.8) and (1.9) simplifies the rotor operator of (1.4)

$$\mathbf{rot} = \begin{bmatrix} 0 & -\partial/\partial z & 0 \\ -\partial/\partial z & 0 & i\zeta \\ 0 & -i\zeta & 0 \end{bmatrix}. \quad (1.12)$$

The possibility of using a 4 x 4-matrix method to study the reflection and transmission of polarized light by anisotropic planar structures is a consequence of the special form assumed by the curl operator in eq. (1.12). In particular, if eq. (1.12) is substituted into eq. (1.1), the resulting operator \mathbf{O} generates two linear homogeneous algebraic equations and four linear homogeneous first-order differential equations in the six components of Γ when eq. (1.8) is expanded. The two linear homogeneous algebraic equations can be solved for the field components $E_z(\Gamma_3)$ и $H_z(\Gamma_6)$ along the z-axis in terms of the other four field components $E_x(\Gamma_1)$, $E_y(\Gamma_2)$, $H_x(\Gamma_4)$, $H_y(\Gamma_5)$, along the x- and y-axes. The values E

z and H_z thus obtained are subsequently substituted into the remaining four differential equations to produce four linear homogeneous first-order differential equations in the four field variables E_x, E_y, H_x, H_y . These can be cast in 4×4 matrix form as follows

$$\frac{\partial}{\partial z} \begin{bmatrix} E_x \\ H_y \\ E_y \\ -H_x \end{bmatrix} = -i\omega \begin{bmatrix} \Delta_{11} & \Delta_{12} & \Delta_{13} & \Delta_{14} \\ \Delta_{21} & \Delta_{22} & \Delta_{23} & \Delta_{24} \\ \Delta_{31} & \Delta_{32} & \Delta_{33} & \Delta_{34} \\ \Delta_{41} & \Delta_{42} & \Delta_{43} & \Delta_{44} \end{bmatrix} \begin{bmatrix} E_x \\ H_y \\ E_y \\ -H_x \end{bmatrix}, \quad (1.13)$$

$$\frac{\partial \psi}{\partial z} = -i\omega / c \Delta \psi. \quad (1.14)$$

Equation (1.14) is the wave equation for the 4×1 generalized field vector

$$\psi = \begin{bmatrix} E_x \\ H_y \\ E_y \\ -H_x \end{bmatrix} \quad (1.15)$$

Δ define a 4×4 differential propagation matrix of the medium. The elements of Δ are functions of the elements of the 6×6 optical matrix M obtained by carrying out the operations indicated above. The relations between the elements of Δ and the elements of M are

$$\begin{aligned}
\Delta_{11} &= M_{51} + (M_{53} + \eta)A_1 + M_{56}A_5 \\
\Delta_{12} &= M_{55} + (M_{53} + \eta)A_4 + M_{56}A_8 \\
\Delta_{13} &= M_{52} + (M_{53} + \eta)A_2 + M_{46}A_6 \\
-\Delta_{14} &= M_{54} + (M_{53} + \eta)A_3 + M_{56}A_7 \\
\Delta_{21} &= M_{11} + M_{13}A_1 + M_{16}A_5 \\
\Delta_{22} &= M_{15} + M_{13}A_4 + M_{16}A_8 \\
\Delta_{23} &= M_{12} + M_{13}A_2 + M_{16}A_6 \\
-\Delta_{24} &= M_{114} + M_{13}A_3 + M_{16}A_7 \\
-\Delta_{31} &= M_{41} + M_{43}A_{11} + M_{46}A_5 \\
-\Delta_{32} &= M_{45} + M_{43}A_4 + M_{46}A_8 \\
-\Delta_{33} &= M_{42} + M_{43}A_2 + M_{46}A_6 \\
\Delta_{34} &= M_{44} + M_{43}A_3 + M_{46}A_7 \\
\Delta_{41} &= M_{21} + M_{23}A_1 + (M_{26} - \eta)A_5 \\
\Delta_{42} &= M_{25} + M_{23}A_{14} + (M_{26} - \eta)A_8 \\
\Delta_{43} &= M_{22} + M_{23}A_2 + (M_{26} - \eta)A_6 \\
-\Delta_{44} &= M_{24} + M_{23}A_3 + (M_{26} - \eta)A_7
\end{aligned} \tag{1.16}$$

Where

$$\begin{aligned}
A_1 &= (M_{61}M_{36} - M_{31}M_{66}) / D \\
A_2 &= [(M_{62} - \eta)M_{36} - M_{32}M_{66}] / D \\
A_3 &= (M_{64}M_{36} - M_{34}M_{66}) / D \\
A_4 &= [M_{65}M_{36} - (M_{35} + \eta)M_{66}] / D \\
A_5 &= (M_{63}M_{31} - M_{33}M_{61}) / D \\
A_6 &= [M_{63}M_{32} - (M_{62} - \eta)M_{33}] / D \\
A_7 &= (M_{63}M_{34} - M_{33}M_{64}) / D \\
A_8 &= [(M_{35} + \eta)M_{63} - M_{33}M_{65}] / D \\
D &= M_{33}M_{66} - M_{36}M_{63} \\
\eta &= \zeta / \omega = N_0 \sin \varphi_0 / c
\end{aligned} \tag{1.17}$$

Recall that the 6×6 optical matrix M is structured from the permittivity ε , permeability μ and optical-rotation ρ , $n\rho$ tensors, according to the equations(1.6). From ε , μ , ρ , $n\rho$ and η , the differential propagation matrix Δ can be calculated using eqs. (1.16) and (1.17). With Δ known, the law of propagation (wave

equation) for the generalized field vector ψ (or, equivalently, its elements, the components of \mathbf{E} and \mathbf{H} parallel to the x- and y-axes) is specified by eq. (1.14).

Let us consider an anisotropic medium bounded by isotropic substrates with refractive indices n_1 and n_2 of the input and output media, respectively. Using the matching conditions, we can calculate three generalized field vectors for the incident, reflected, and transmitted plane waves

$$\psi_i = \begin{bmatrix} E_x \\ n_1 E_x / \cos(\alpha_1) \\ E_y \\ n_1 E_x \cos(\alpha_1) \end{bmatrix} \quad (1.18)$$

$$\psi_r = \begin{bmatrix} R_x \\ -n_1 R_x / \cos(\alpha_1) \\ R_y \\ -n_1 R_x \cos(\alpha_1) \end{bmatrix} \quad (1.19)$$

$$\psi_t = \begin{bmatrix} T_x \\ n_2 T_x / \cos(\alpha_2) \\ T_y \\ n_2 T_x \cos(\alpha_2) \end{bmatrix} \quad (1.20)$$

Here α_1 and α_2 are angles of the light beam in the input and output media. The relation between the parameters is $n_1 \sin(\alpha_1) = n_2 \sin(\alpha_2)$.

The reflection and transmission coefficients can be calculated by:

$$T = \frac{n_2 \cos(\alpha_2) |T_x / \cos(\alpha_2)|^2 + |T_y|^2}{n_1 \cos(\alpha_1) |E_x / \cos(\alpha_1)|^2 + |E_y|^2} \quad (1.21)$$

$$R = \frac{|R_x / \cos(\alpha_1)|^2 + |R_y|^2}{|E_x / \cos(\alpha_1)|^2 + |E_y|^2} \quad (1.22)$$

2. Photonic defect modes in cholesteric liquid crystal with a resonant nanocomposite layer

2.1. Optics of CLCs with defect of structure

Introducing various types of defects into the structure of an ideal cholesteric makes it possible to obtain narrow transmission bands in PC bandgaps that will correspond to localized defect modes. These modes, similarly to defect modes in scalar periodic layered media, can be used to produce narrowband and tunable filters [18], optical diodes [19], liquid crystal rotator and a tunable polarizer [20], polarization azimuth rotation and azimuth stabilizers [21] and other devices. Low threshold laser generation in CLC is under extensive research [22]. There are two possible options of such generation: band edge lasing [23] and defect mode lasing [24].

There exist a few ways of inducing photonic defect modes in CLC. This can be achieved by using a thin layer of isotropic [25] or anisotropic substance confined between two layers of CLC [26,27], twist-defect (jump of the rotation angle of the cholesteric helix) [28-30] or defect associated with local changes in the helix pitch [30-32]. The authors of [33], using an analytical approach to the theory of optical defect modes in CLC with an isotropic defect layer, developed a model that isolates polarization mixing and yields light equation only for diffractive polarization. Analysis of defect modes in CLC induced by twist defect, i.e. by a sharp turn of the director around the CLC axis at the interface of two CLC layers, can be found in [34,35]. The direction of predominant orientation of molecules in CLC is referred to as a CLC director. Propagation of light in CLC containing a dielectric layer combined with twist-defect at the interface between the dielectric and CLC layer was studied in [18,36]. PCs doped with substances having strong optical resonance are under extensive research. An example of a giant optical resonance has been predicted for a nanocomposite (NC) consisting of metallic nanoballs dispersed in a transparent

matrix [37,38] while the optical characteristics of primary materials lack resonant properties. The resonance is characterized by effective permittivity in approximation of the Maxwell Garnett formula, which is proved by both the numerical simulation [39] and experiment [40]. The effective characteristics of a NC containing metallic nanoparticles dispersed in a dielectric matrix are due to the plasmon resonance of nanoparticles. These characteristics can have unique magnitudes not inherent in natural materials. For instance, the effective refractive index can be in excess of 10. Dispersion of resonant medium combined with the PC dispersion provides a new tool to control spectral and optical properties of PCs [41-45].

The chapter is focused on spectral properties of CLC with a combined defect. A NC layer with resonance dispersion and a phase jump at the interface between the NC and CLC layers serve as such a defect. Splitting of the defect mode and localization of the electromagnetic field are analyzed depending on the volume fraction of nanoparticles in the defect layer. Phase jump of the CLC helix in the transmission spectrum is discussed. We also study modification of the transmission spectrum of cholesteric with a combined defect under external fields affecting the CLC helix pitch.

2.2. Isotropic nanocomposite defect layer

The PC structure under consideration consists of two identical layers of CLC with a right-handed twist separated by a NC defect layer combined with a twist defect (Figure 2.1). The length of the entire structure is $L = 2.946 \mu\text{m}$, the CLC helix pitch is $p = 275 \text{ nm}$, and the defect layer thickness is $d = 196 \text{ nm}$. The medium outside CLC is isotropic and has the refractive index $n = (n_o + n_e)/2$, where $n_o = 1.4$ and $n_e = 1.6$ are the ordinary and extraordinary refractive indexes of cholesteric, respectively. For the chosen external medium, Fresnel reflection from the CLC surface and interference processes from the boundary surfaces will be weak. The twist defect magnitude is governed by the angle α that is positive when the vector tip of the CLC director rotates clockwise at the interface between NC and CLC layers (conventionally observed along the direction of light propagation).

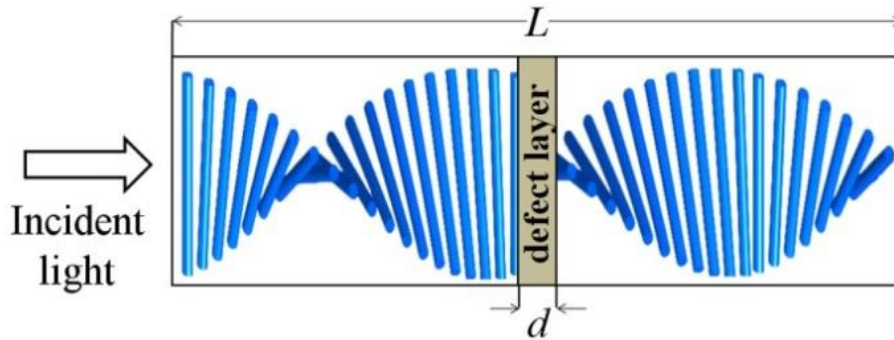


Figure 2.1. Schematic of CLC with a combination of defects

The effective permittivity of a NC layer ϵ_{mix} is found from the Maxwell Garnett formula widely used when dealing with matrix media where a small volume fraction of isolated inclusions is dispersed in the material matrix [46,47]:

$$\epsilon_{mix} = \epsilon_d \left[\frac{f}{(1-f)/3 + \epsilon_d / (\epsilon_m - \epsilon_d)} + 1 \right]. \quad (2.1)$$

Here f is the filling factor, i.e. the fraction of nanoparticles in the matrix, ε_d and $\varepsilon_m(\omega)$ are the permittivities of the matrix and the metal of nanoparticles, respectively, ω is the radiation frequency. The size of nanoparticles is much smaller than the wavelength and the depth of field penetration into the material. Find permittivity of the metal of nanoparticles using the Drude approximation:

$$\varepsilon_m(\omega) = \varepsilon_0 - \frac{\omega_p^2}{\omega(\omega + i\gamma)}, \quad (2.2)$$

where ε_0 is the background dielectric constant taking into account contributions from interband transitions, ω_p is the plasma frequency, γ is the plasma relaxation rate[48]. For silver nanoballs dispersed in a transparent optical glass, $\varepsilon_0 = 5$, $\hbar\omega_p = 9$ eV, $\hbar\gamma = 0.02$ eV, $\varepsilon_d = 2.56$.

Ignoring the small factor γ^2 , we find position of the resonant frequency that depends on the characteristics of primary materials and the dispersed phase concentration f .

$$\omega_0 = \omega_p \sqrt{\frac{1-f}{3\varepsilon_d + (1-f)(\varepsilon_0 - \varepsilon_d)}}. \quad (2.3)$$

Figure 2.2 shows dispersion dependence of the nanocomposite permittivity for two different filling factors: $f = 0.02, 0.1$. As can be seen in the figure, the ω_0 frequency corresponding to resonance in the defect layer shifts towards the long-wavelength range of the spectrum with the growing concentration of nanoballs. Note that the resonant curve half width ε''_{mix} is very little affected while the ε'_{mix} curve is essentially modified and the range of frequencies increases for which the NC is similar to metal when $\varepsilon'_{mix} < 0$.

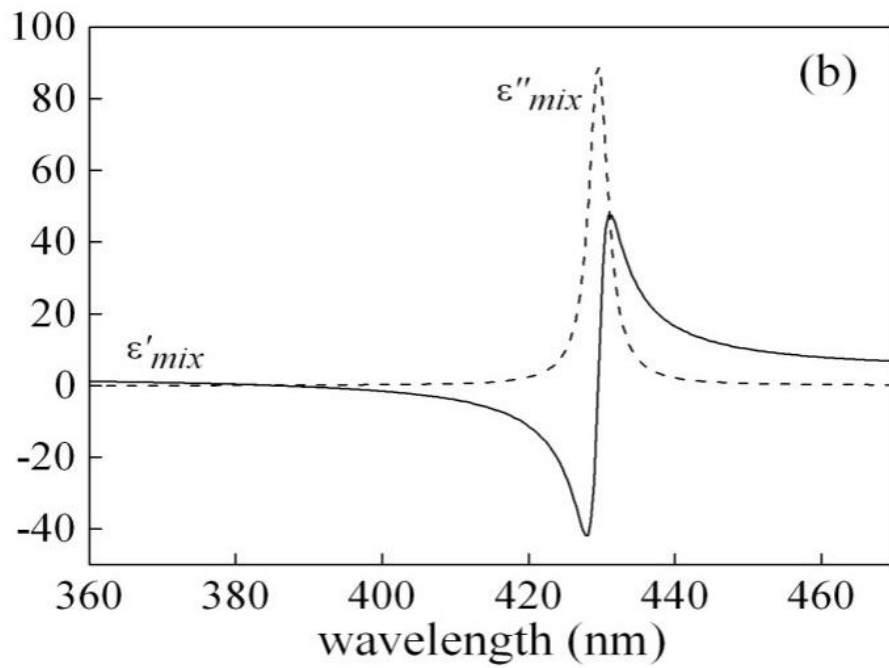
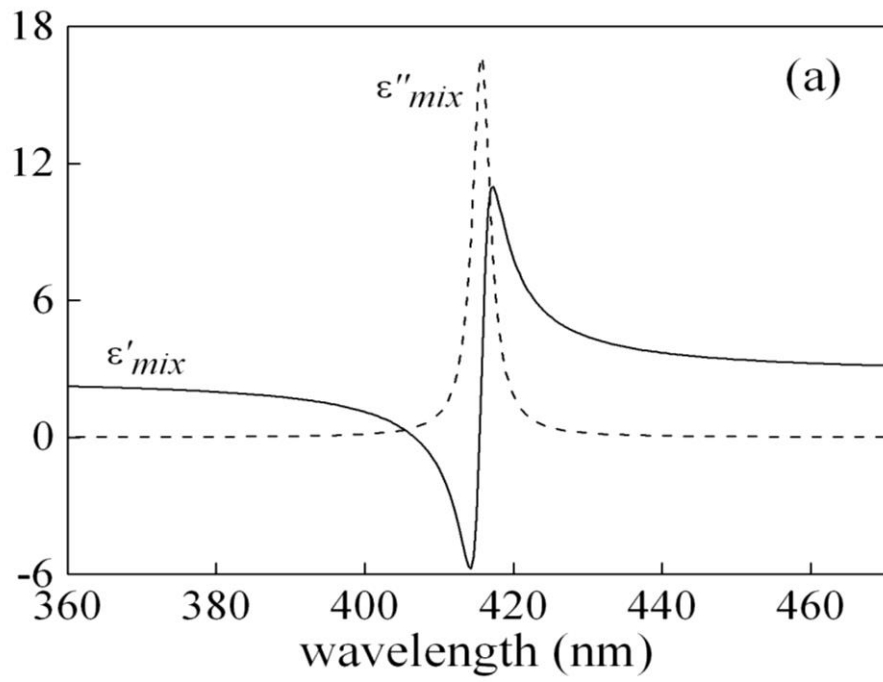


Figure 2.2. Imaginary ϵ''_{mix} (dashed curve) and real ϵ'_{mix} (solid curve) parts of the effective permittivity of ϵ_{mix} versus wavelength. The filling factor $f = 0.02$ (a), 0.1 (b)

The proposed system can be fabricated according to the procedure described in [49]. Difficulty may be due to the small thickness of the

nanocomposite layer. When assembling cell nanocomposite layer is in contact with the oriented CLC layers. Non-contact method is preferred for orientant applying. Wide annular spacers are required to ensure the flatness of a thin layer of nanocomposite. Manipulation of the CLC optical characteristics by means of electrical, magnetic, optical fields or temperature is well known and robust technique.

2.3. Transmission spectra of CLC with isotropic resonance defective nanocomposite layer

Figure 2.3 shows the seed ($f = 0$) transmission spectrum on the normal incidence of light onto a cholesteric with a defect of the structure in the form of a dielectric plate without twist-defect ($\alpha=0$). It is readily seen from the figure that, like in [25], the photonic band gap has peaks corresponding to defective modes of the CLC, which are induced for both circular polarizations of normally incident light. In addition, the defective modes have the same wavelength and the same transmittivity.

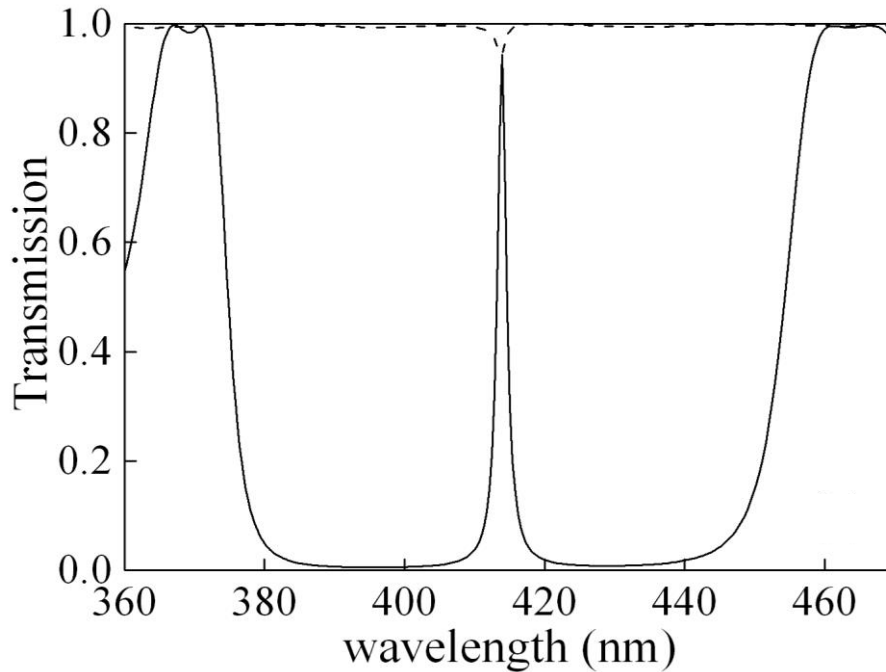


Figure 2.3. Transmission spectrum for right- (solid curve) and left-handed (dashed curve) polarizations for $\alpha = 0, f = 0$

If the filling factor is nonzero and the resonance frequency ω_0 of the nanocomposite coincides with the defective mode frequency, the defective mode frequency is split by analogy with the splitting of the frequencies of two coupled oscillators. The manifestation of the splitting in the transmission, reflection, and

absorption spectra is illustrated by Figure 2.4. It is evident from Figure 2.4a that, as a result of splitting, the defective modes for the right and left-handed circular polarizations have the same wavelength but different transmittivities at the center of the peak. The computations show that, as like as in a scalar onedimensional PC with a defective nanocomposite layer [41], the splitting increases with the volume fraction of nanoballs in the composite.

For the reflection and absorption spectra (Figures 2.4b, 2.4c), a strong dependence of the reflection and absorption coefficients on the direction of the circular polarization of incident light is typical.

The emergence of two defective modes in the spectral range forbidden for both polarizations after the splitting (Figure 2.4a) is connected, primarily, with the substantial reflection and absorption of waves of the right-hand left-handed circular polarizations, respectively, (Figures 2.4b, 2.4c).

The result of the twist-defect is the repositioning of defect modes in the bandgap of CLC, which affects transmission at the defect mode frequency. Figure 4a shows that clockwise rotation of the second CLC layer ($\alpha > 0$) makes both peaks corresponding to defect modes for right-handed and left-handed polarizations shift to the shorter wavelength range. Transmittance of the long-wavelength peak drops down with the growing α , whereas that of the short-wavelength peak enhances.

A reverse situation is observed when the CLC layer is rotated anti-clockwise ($\alpha < 0$) (Figure 2.5b). Redistribution of transmission intensity at defect modes depending on α is obviously associated with their coupling due to the twist defect. No defect modes of either polarization emerge in the bandgap zone of CLC for the chosen parameters of the system and $\alpha = \pi/2$. Our calculations show that peaks for light of non-diffractive polarization are not observed just for any α . The bandgap location is almost independent of the twist defect magnitude.

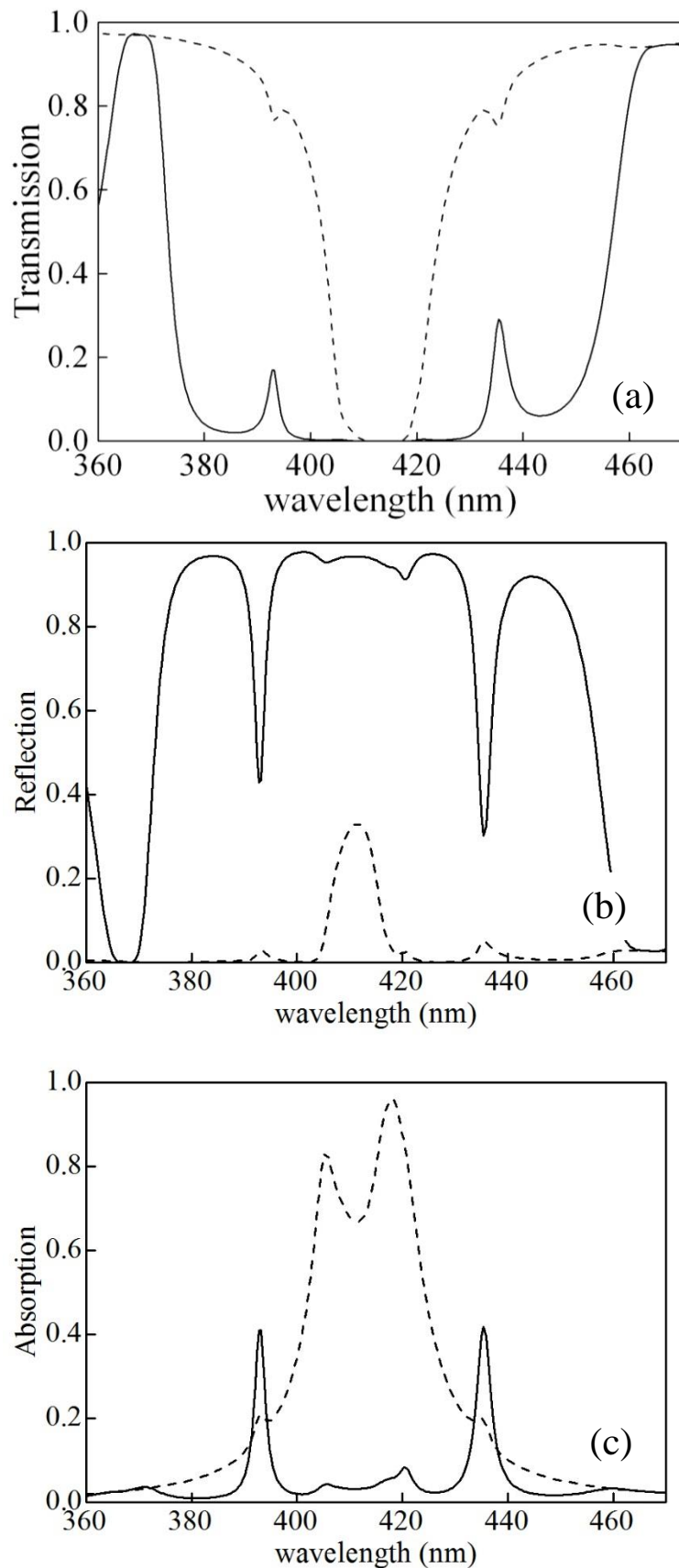


Figure 2.4. (a) Transmission, (b) reflection, and (c) absorption spectra for waves with the right-handed (solid line) and left-handed (dashed line) circular polarizations, $\theta = 0^\circ$. The filling factor is $f = 0.02$.

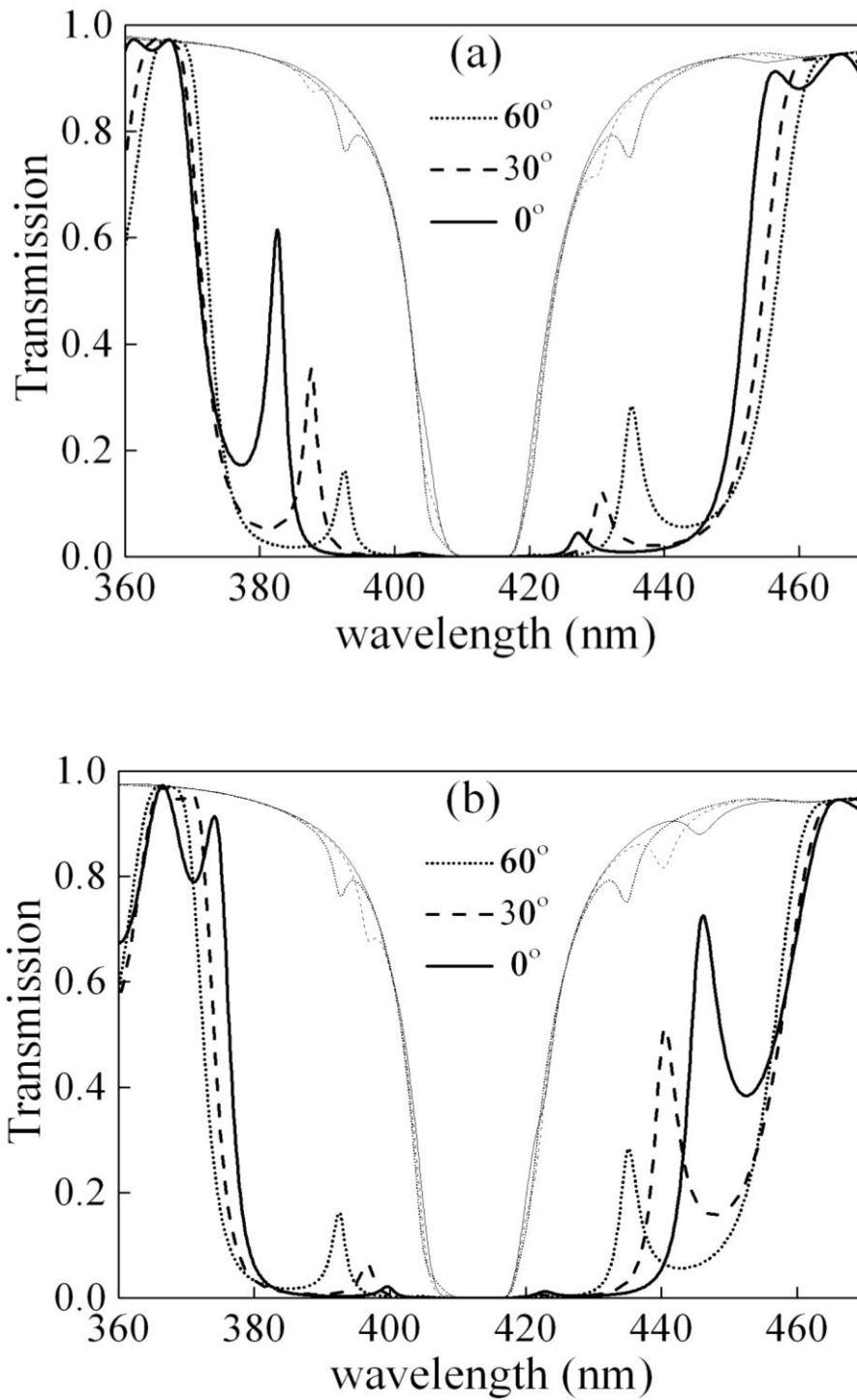


Figure 2.5. Transmission spectra of the structure for various α : (a) $\alpha > 0$, (b) $\alpha < 0$. Bold curves refer to the right-handed and thin curves to left-handed circular polarizations of light $f = 0.02$.

Figure 2.6 is an example of spatial distribution of electric field in $\lambda = 388.2$ nm defect modes for $\alpha = 30^\circ$ (see Figure 2.5a). Field localization is

most prominent in the area comparable with the wavelength for the mode corresponding to diffractive polarization.

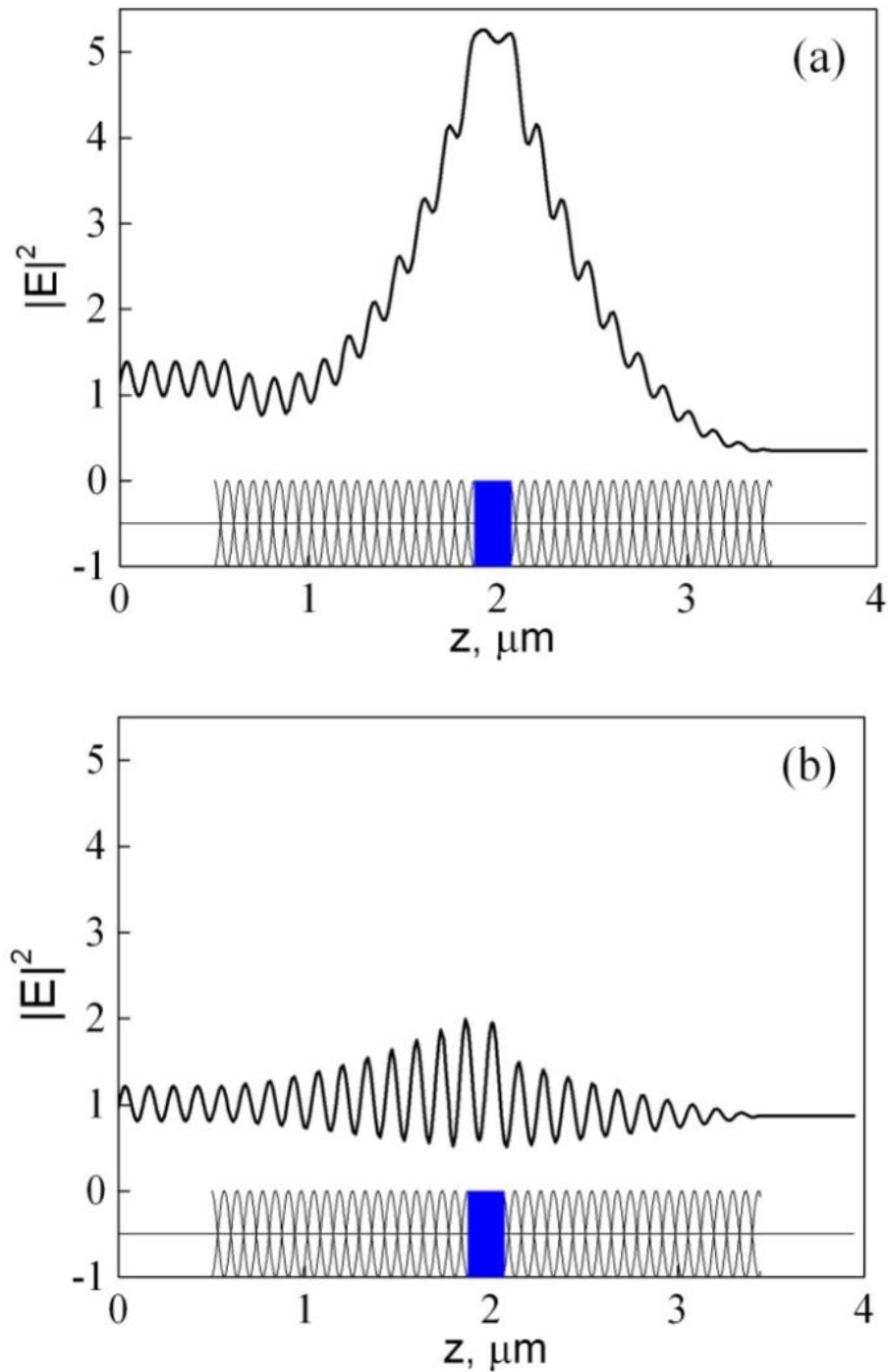


Figure 2.6. Distribution of the squared electric field modulus in defect modes with $\lambda = 388.2$ nm (Option 3 in Figure 2.5a). (a) Wave with right-handed circular polarization, (b) Wave with left-handed circular polarization. $f = 0.02$.

Note that an increase in the number of periods of a cholesteric helix leads to an increase in the photonic band gap slope. In addition, the transmission peaks corresponding to the waves with the right-hand diffracting and left-hand circular polarization of light decrease for a defect with a factor of $f=0$ (Fig. 3.3). This behavior of the defect mode peaks with increasing number of cholesteric periods is observed also in our case, when the factor of nanocomposite filling with metal particles is nonzero. In particular, at $f=0.02$, $\alpha=0$ (Fig. 3.4), and 30 CLC periods on the left and on the right from the defect (the total thickness of the structure with the defect is $16.696 \mu\text{m}$), the peak transmittances for the diffraction polarization of light become almost zero. However, the peak transmittances for the left-hand polarization of light are 0.68 and 0.67, respectively.

2.4. Controlling of transmission spectrum of CLC with combined defect layer

By varying the CLC helix pitch p and the angle of light incidence on the sample it is possible to control the transmission spectrum behavior. Increasing the helix pitch, for example by varying the temperature, results in a bandgap shift to the long-wavelength region following the Bragg condition $pn = \lambda$. The short-wavelength peak corresponding to the defect mode disappears; the long-wavelength peak of defect modes corresponding to the right- and left-handed circular polarizations remains. It is essential that there are pitches for which the resonance frequency ω_0 appears to be located close to the short-wavelength boundary of band gap.

An example of the resultant changes in the transmission spectrum of the structure at $\alpha = -30^\circ$ is illustrated in Fig. 6a. The CLC helix pitch was changed from $p = 275\text{nm}$ to $p = 305\text{ nm}$, which made the NC resonant frequency ω_0 move close to the short-wavelength boundary of band gap.

Bandgap splitting is observed when the resonance mode is coupled with photonic modes. An extra transparency band induced by diffractive polarization splits off the short-wavelength edge to give rise to a bandgap in the vicinity of ω_0 for waves of both polarizations. The stop band is primarily the result of field absorption in the NC layer. A further increase of the helix pitch forces the resonant frequency ω_0 to shift to the continuous transmission spectrum. The developed resonance situation in this case facilitates formation of an extra bandgap in the transmission spectrum (Fig. 6b).

An alternative approach to realize similar effects is to increase the angle of light incidence on the structure. Then, following the Bragg condition, the bandgap will shift toward the short-wavelength range while the long-wavelength edge of band gap comes closer to the resonant frequency ω_0 of the defect layer.

As mentioned above, high susceptibility to external fields is an essential advantage of CLC over other types of PCs. These fields can be used to control

the helix pitch not only of the entire cholesteric but also of part of CLC on the left or on the right of the defect. Consider transmission spectra behavior of the structure when the CLC helix pitch is changed on the right of the defect p_2 . First we analyze an initial structure of two CLC layers coupled with dielectric defect.

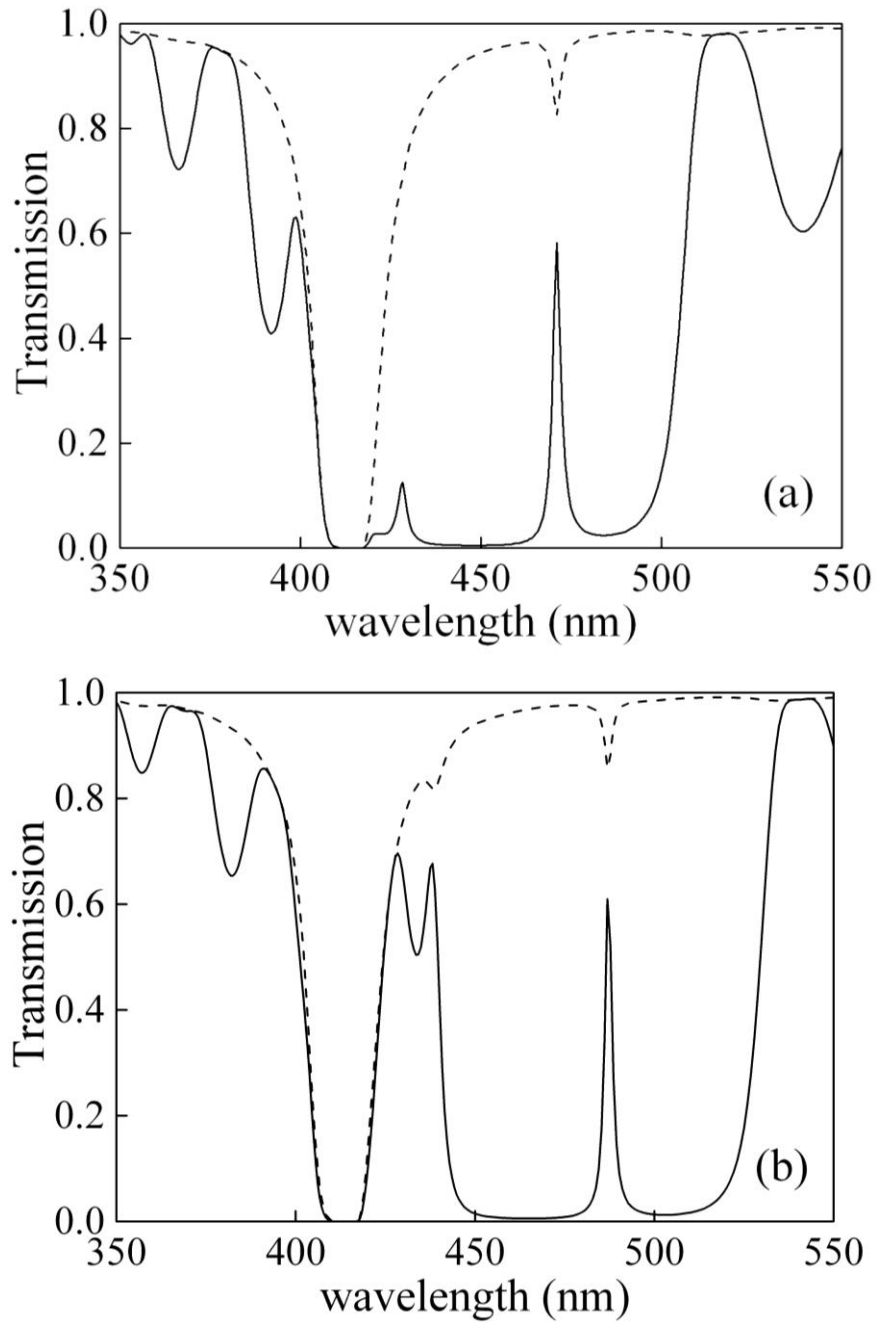


Figure 2.7. Transmission spectrum for various helix pitches. (a) $p = 305$ nm, (b) $p = 320$ nm. Solid and dashed curves refer to the right-handed and left-handed circular polarizations of light, respectively. $f = 0.02$, $\alpha = -30^\circ$.

Transmission spectrum of the structure is shown in Fig. 3a. There is no twist defect in this case, $\alpha = 0$ and the filling factor is $f = 0$. Figure 7a shows the transmission spectra for two individual CLC layers with various helix pitches, and for a system of these CLC layers separated by a defect.

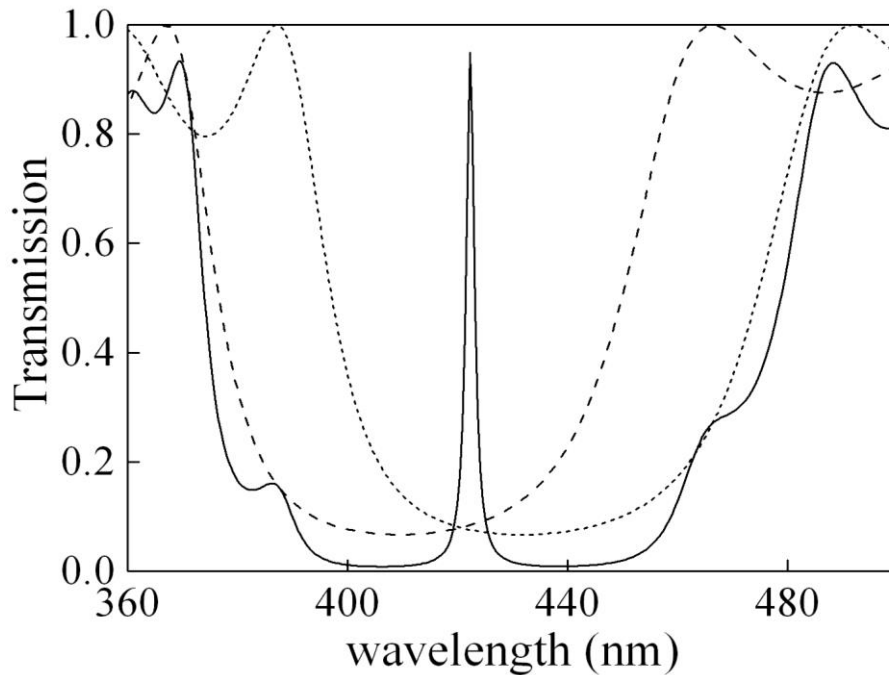


Figure 2.8. Transmission coefficient for a system of two cholesterics with a defect (solid curve) and for each of the cholesterics (dashed curve) with the pitch on the left of the defect $p_1 = 275$ nm (cyan dotted curve) and $p_2 = 290$ nm (red dotted curve). The remaining parameters are the same as in Figure 2.3.

In the figure we can see that the defect mode occurs in the area where bandgaps of the two CLCs overlap. Our calculations show that the greater the pitch of the right-side helix, the broader the band gap of the system. This fact of band gap broadening and occurrence of a defect mode in the region of overlapping of two scalar PCs was used to obtain a tunable asymmetric filter in a recent experiment [50].

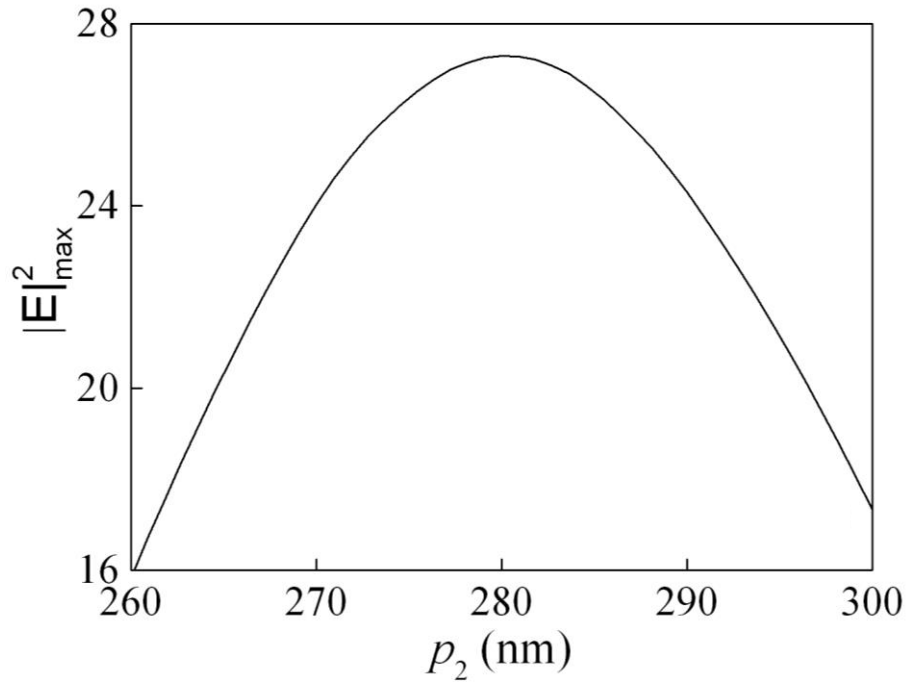


Figure 2.9. Maximum squared modulus of the electric field of the defect mode as a function of the pitch p_2 . The remaining parameters are the same as in Figure 2.3.

The defect mode is shifted to the long-wavelength range of the spectrum as the right-side helix pitch grows, which results in a lower transmission coefficient in the maximum of the defect mode band. When p_2 is not sufficient for bandgaps of the two CLCs to overlap, there is no defect mode realized. Note also the nonmonotonous behavior of the squared modulus maximum of the electric field in a localized defect mode observed as the pitch p_2 grows (Figure 2.9). Figures 2.10, 2.11 illustrates the behavior of the transmission spectrum and squared field modulus of a long-wavelength defect mode for various pitches p_2 when $\alpha = -30^\circ$, $f = 0.02$, other parameters of the system being the same. Broadening of band gap width is observed as the pitch p_2 grows. (Figure 2.10). Moreover, the maximum of the squared field modulus localized in the defect mode is shifted due to the twist defect (Figure 2.11).

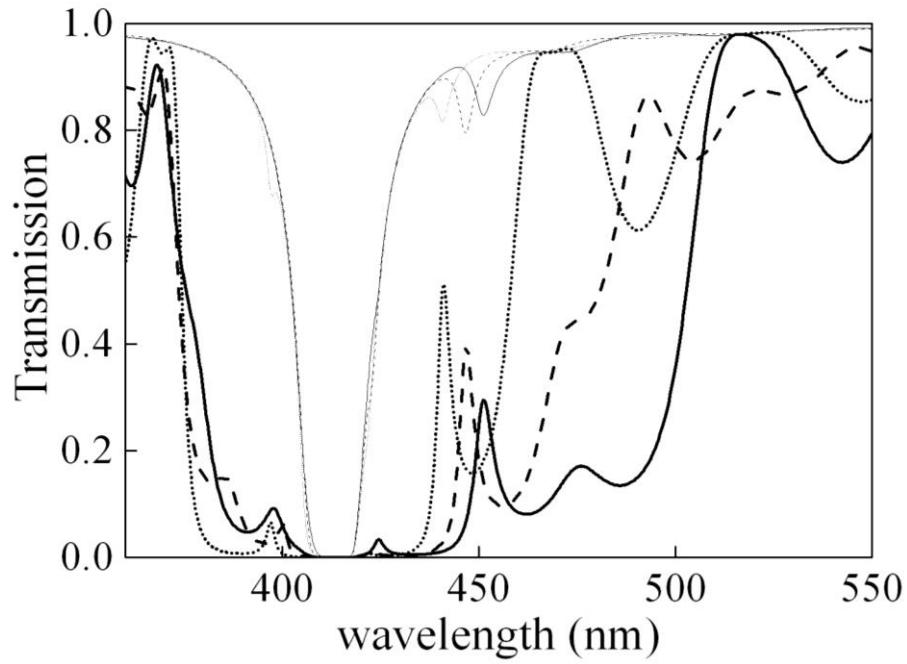


Figure 2.10. Transmission spectra for various p_2 : Solid curve $p_2 = 275$ nm, dashed curve $p_2 = 290$ nm, dash-and-dotted curve $p_2 = 305$ nm, $\alpha = -30^\circ$.

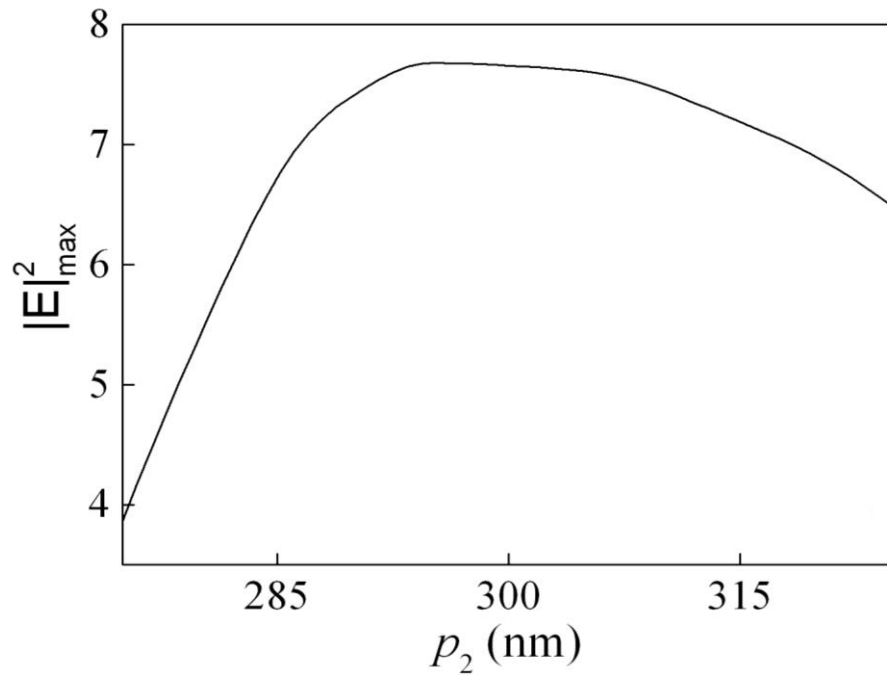


Figure 2.11. Maximum of the squared electric field modulus of the long-wavelength defect mode as a function of the pitch p_2 , $\alpha = -30^\circ$. Bold curves refer to the right-handed and thin curves to the left-handed circular polarizations of light, $f = 0.01$

3. Optical localized states in structures containing cholesteric liquid crystal

3.1 Surfaceelectromagneticwaves

Special localized modes called the surface states can exist between different media. The surface states in photonic crystal media are promising objects for fundamental research and application [51]. Such localized modes at the interface between two highly reflective materials can be formed by both the TE and TM linear polarizations and excited at any angles of light incidence. At normal incidence, such states are often called Optical Tamm States (OTS) [52]. They are realized when light is locked between two mirrors, for example, at the boundary of a photonic crystal (PC) and other PC [53], or between a PC and a medium with the negative permittivity [54, 55]. Recently, the OTS has been obtained at the interface between a one-dimensional PC and organic dye-doped polymer layer [56]. The localized modes manifests itself in experiments as a narrow resonance in the transmission or reflection spectrum of a sample [57,58].

The surface modes and OTSs are promising for application in sensors [59,60], bistable switches [61,62], Faraday- and Kerr-effect amplifiers [58, 63], organic solar cells and photovoltaic elements [64-66], absorbers [67] and top-emitting white organic light-emitting devices [68]. The authors of study [69,70] experimentally demonstrated a laser based on the Tamm structure consisting of quantum wells embedded in a Bragg reflector with the silver-coated surface. Gazzano et al. experimentally showed the possibility of implementation of a single-photon source on the basis of confined Tamm plasmon modes [71]. The optical Tamm states in magnetophotonic crystals were investigated in studies [58, 72–74]. The hybrid states were studied in [75–80]. In [81], the electro-optically tunable Tamm plasmon exciton polaritons were investigated. The authors of [82] predicted that the edges of a finite one-dimensional array of

dielectric nanoparticles with the high refractive index can support evanescent OTSs.

The authors of [83] proposed and implemented the extremely high-efficiency transmission of light through a nanohole in a gold film, which was placed in the light field localized at the interface between the film and a one-dimensional photonic crystal. This effect is related to the field amplification at the interface between the superlattice and the metal film due to the occurrence of the OTS.

The chapter describe possibilities for light localization at the interface between the CLC and metallic layer. This problem is nontrivial due to the polarization features of light reflection from the CLC and metal [84,85]. The light reflected from the CLC retains its circular polarization, but the metal changes it. The polarization change can be compensated using an additional anisotropic layer. The role of such a layer was played by a quarter-wave plate inserted between the CLC and metal [84], by an oppositely handed CLC [86], or defect-containing CLC [87]. One more way to find the OTS at the CLC boundary was the use of a chirality-preserving mirror instead of the metal [88, 89].

3.2. Localized Optical States in a ‘photonic cholesteric liquid crystal – phase plate – metal’ structure

3.2.1. Surface localized modes

The investigated structure consists of a thin right-hand CLC layer, a quarter-wave anisotropic plate, and a metal film (figure 1). The plate is cut parallel to the optical axis and shifts the wave phase by $\pi/2$. At the interface between the CLC and the phase plate, the cholesteric director, i.e., the preferred direction of molecules, is oriented along the optical axis. The CLC layer thickness is $L = 2 \mu\text{m}$, the helix pitch is $p = 0.4 \mu\text{m}$, and the ordinary and extraordinary refractive indices are $n_o = 1.4$ and $n_e = 1.6$, respectively. The phase plate thickness is $d = 0.75 \mu\text{m}$ and its refractive indices are $n'_o = n_o$ and $n'_e = n_e$. The parameters of the phase plate satisfy the relation

$$2\pi(n'_e - n'_o)d/\lambda = \pi/2 \quad (3.1)$$

The phase plate is coupled with a silver film with the thickness $d_m = 50 \text{ nm}$. The permittivity of the metal is specified in the form of the Drude approximation (2.2). The structure is surrounded by a medium with the refractive index n equal to the average refractive index of CLC.

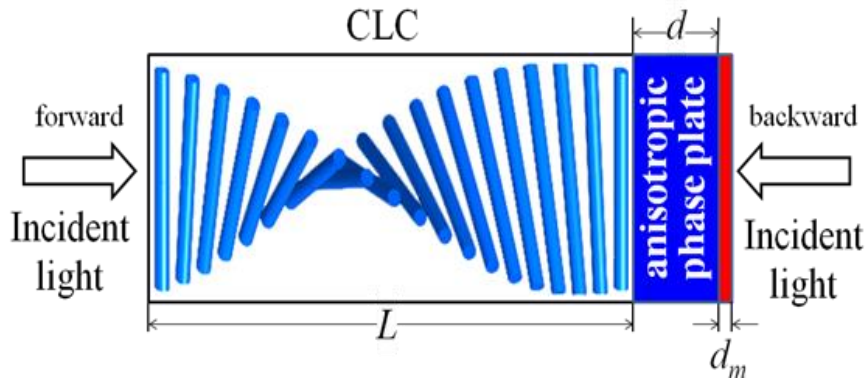


Figure 3.1. Schematic of the ‘CLC– phase plate – metal’ structure.

Figure 3.2 shows the calculated transmission spectra for the diffracting polarization for the CLC, metal layer, and the entire structure. The Bragg reflection region lies between 560 and 640 nm. At these wavelengths, the real part of the permittivity of silver is negative. At the wavelength corresponding to the CLC band gap, a narrow transmission peak is observed.

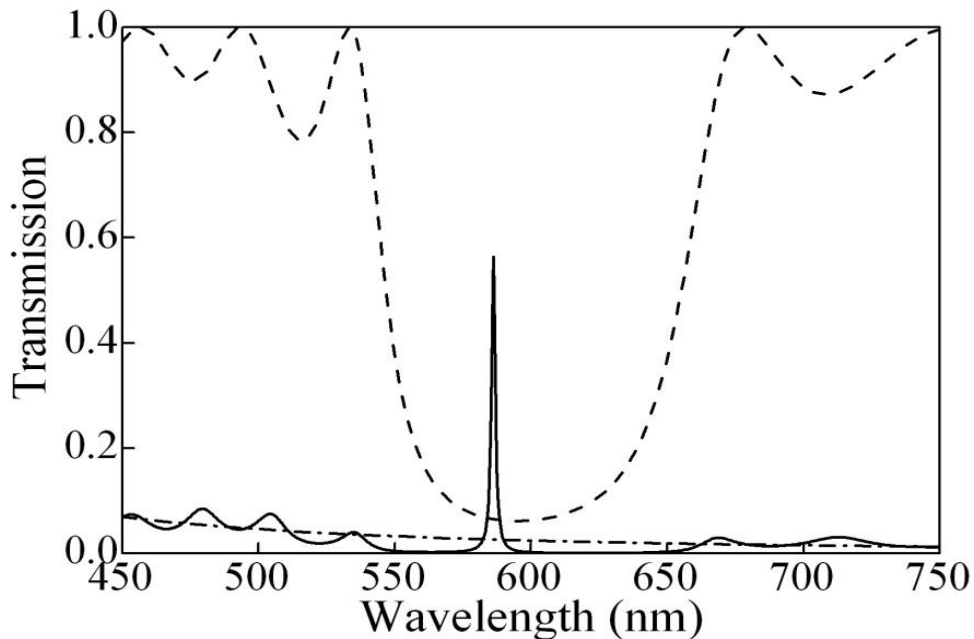


Figure 3.2. Transmission versus wavelength with light incidence normal to CLC (dashed line), to the silver film (dash-dotted line) and to the ‘CLC– phase plate – metal’ structure (solid line).

The electric field intensity distribution in the sample for the diffracting polarization is illustrated in Figure 3.3.

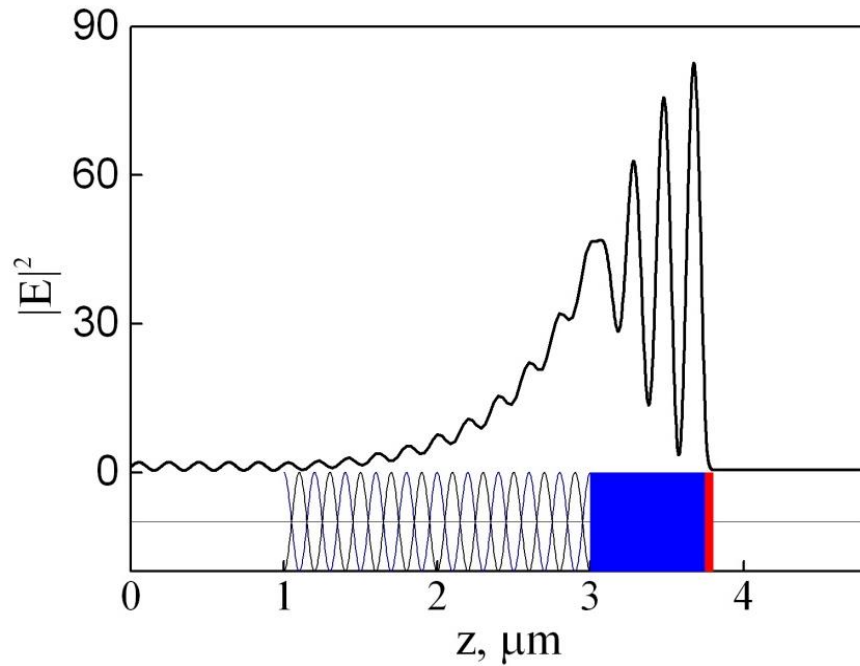


Figure 3.3. Distribution of the squared modulus of the electric field intensity $|E(z)|^2$ in the ‘CLC– phase plate – metal’ structure for $\lambda = 586$ nm. Field is normalized to the input field equal to unity.

The light is localized near the metal film with the maximum electric field value at the interface between the phase plate and metal. The decay of the localized mode field in the metal is caused by the negative permittivity of the metal film, while the decay of this field in the CLC is caused by Bragg reflection at the CLC/plate interface.

Let us consider the occurrence of localization between the CLC and the metal (Figure 3.4). First, we explain why the light cannot be localized between the CLC and the metal without the quarter-wave phase plate.

We will investigate the four cases:

(i) The left-hand circularly polarized light falls on the CLC and freely passes through it. Upon reflection from the metal, the left-hand circular polarization transforms to the right-hand one. Upon reflection from the CLC, the right-hand circular polarization is retained. Upon repeated reflection from the metal, the right-hand circular polarization transforms to the left-hand one and the light propagates through the crystal in the backward direction (Figure 3.4a).

(ii) The right-hand diffracting-polarized light falls on the CLC. A part of the light passed through the CLC retains its polarization, but upon reflection from the metal the right-hand circular polarization transforms to the left-hand one and the light freely passes through the CLC structure in the backward direction (Figure 3.4b).

Let us consider the effect of the quarter-wave plate on the polarization of light.

(iii) The left-hand circularly polarized light falls on the CLC. The light freely passes through the CLC. The light passed through the plate acquires the linear polarization. Upon reflection from the metal, the linear polarization is retained. The light passed through the plate in the backward direction acquires the left-hand circular polarization. After that, the light propagates through the CLC in the backward direction (Figure 3.4c).

(iv) The right-hand diffracting-polarized light falls on the CLC. A part of the light passed through the CLC retains its polarization. The light passed through the plate acquires the linear polarization. Upon reflection from the metal, the linear polarization is retained. The light passed through the plate in the backward direction acquires the right-hand circular polarization. Upon repeated reflection from the CLC, the light retains its right-hand circular polarization (Figure 3.4d). Thus, the light is localized between the CLC and the metal.

It is difficult to form a direct contact between the CLC and the metal. To do so, one should apply orientants in the form of layers of an anisotropic material. The orientant can simultaneously be a quarter-wave phase plate. Varying the thickness of this plate, one can implement the localized state.

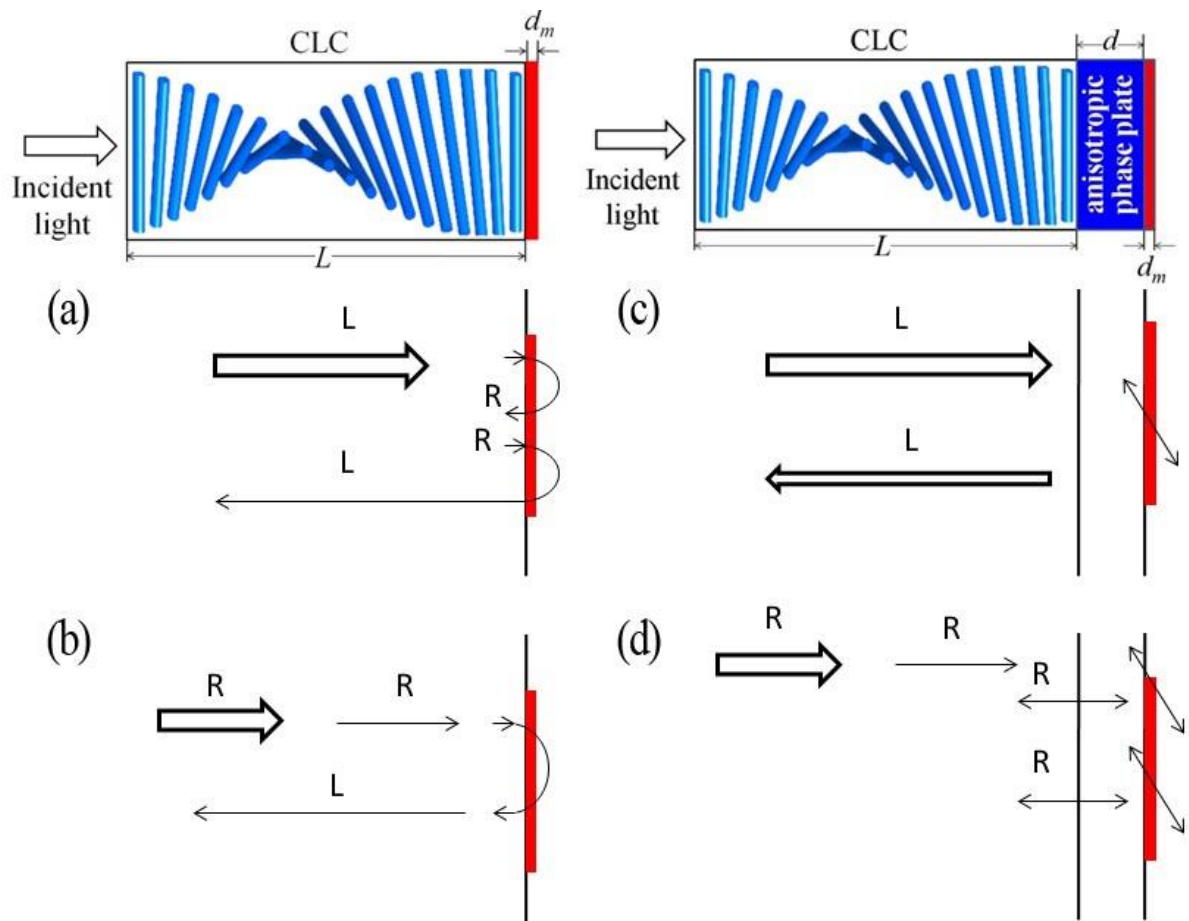


Figure 3.4. Localization of light for right-hand (R) and left-hand (L) polarizations in the structures consisting of (a, b) the CLC and metal layers and (c, d) the CLC layer, phase plate, and metal layer.

To sum up, note that the observed surface state is, in fact, the eigenmode of the microcavity with the CLC layers and metal plane working as mirrors. Consequently, it becomes possible to induce laser generation in a microcavity by using the phase plate from an optically active material.

3.2.2. Transmission anisotropy

For a long time, the cholesteric liquid crystals have been attracting attention of researchers that want to effectively manipulate by light. One of the promising effects in the structures consisting of the CLCs and anisotropic elements is the different transmission spectra for the light of a certain polarization propagating in the forward and backward directions. This phenomenon was demonstrated, in particular, by Hwang et al. [19]. The authors proposed the electric-field-tunable optical diode based on two identically twisted CLCs separated by the nematic liquid crystal layer. As a result, the transmission spectra for the diffracting-polarized light propagating in the forward and backward directions were qualitatively different.

We established that the analogous effect takes place in the investigated model. Figure 3.5 presents the transmission spectra of the structure at the wave incidence on the CLC and on the metal film for the right- and left-hand circularly polarized light.

When the light with the diffracting polarization propagates in the forward direction, the transmittance is 0.57; when the light propagates in the backward direction, the transmittance is 0.34. Thus, we deal with the transmission anisotropy. It was observed that when the left-hand circularly polarized light falls on the structure, the spectrum changes. The transmittances in the forward and backward directions are 0.09 and 0.32, respectively. It should be noted that this effect cannot be implemented in scalar structures.

To elucidate the origin of this effect, we consider the light polarization dynamics at the incidence on the CLC (Figures 3.6a and 3.6b) and on the metal (Figures 3.6c and 3.6d).

When the light with the right-hand diffracting polarization falls on the CLC, a part of the light passed through the crystal approximately retains its polarization at the CLC output. After passing through the quarter-wave plate, the light acquires the linear polarization. The unabsorbed part of light leaves the

metal. Upon reflection from the metal, the linear polarization is retained. After passing through the metal in the backward direction, the light acquires the right-hand circular polarization. Upon repeated reflection from the CLC, the light retains its right-hand circular polarization. Again, the linearly polarized light leaves the metal (Figure 3.6a).

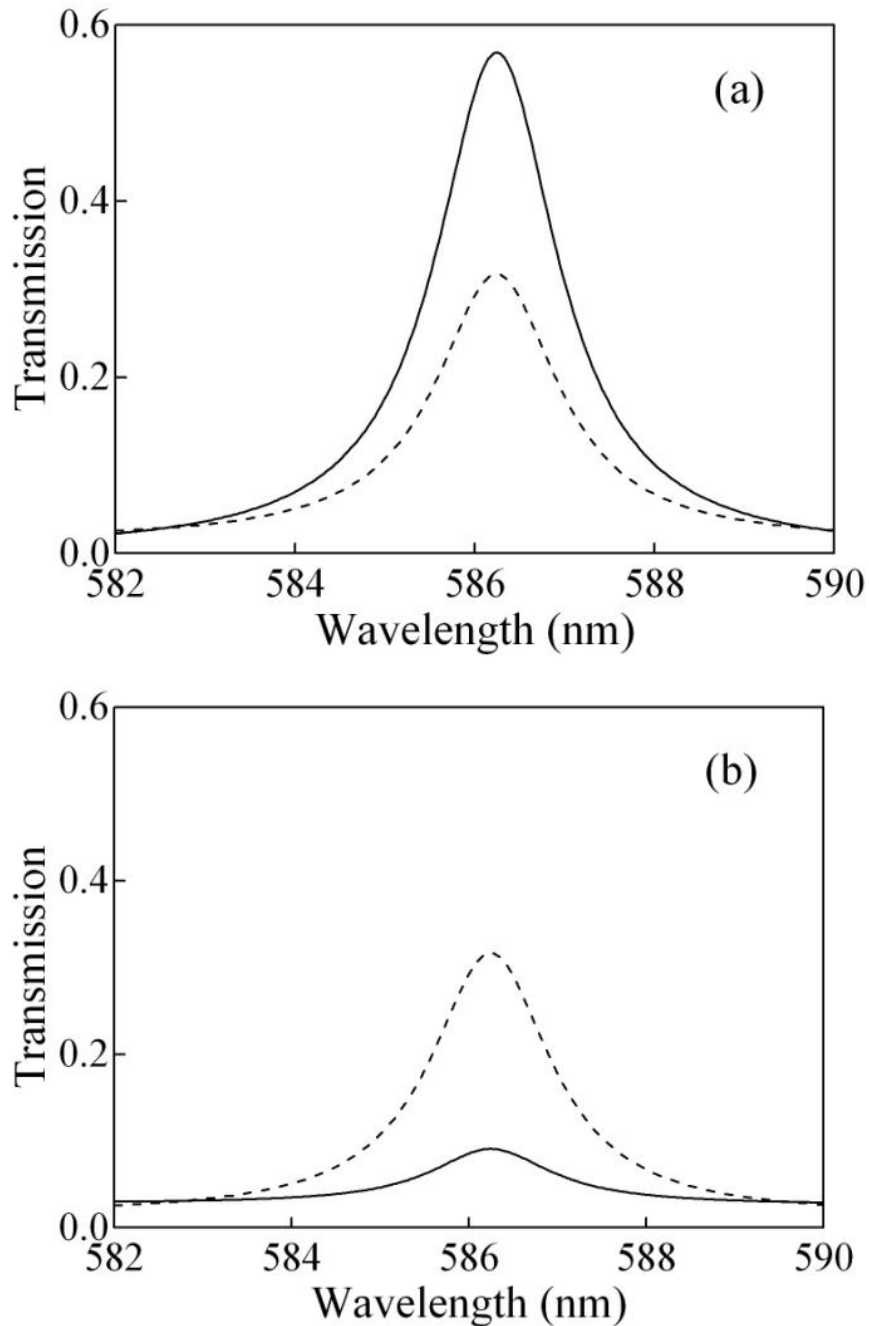


Figure 3.5. Transmission spectrum of the structure for incident waves with (a) the right-hand and (b) left-hand circular polarization. Solid line corresponds to the incidence on the CLC and dashed line, to the incidence on the metal.

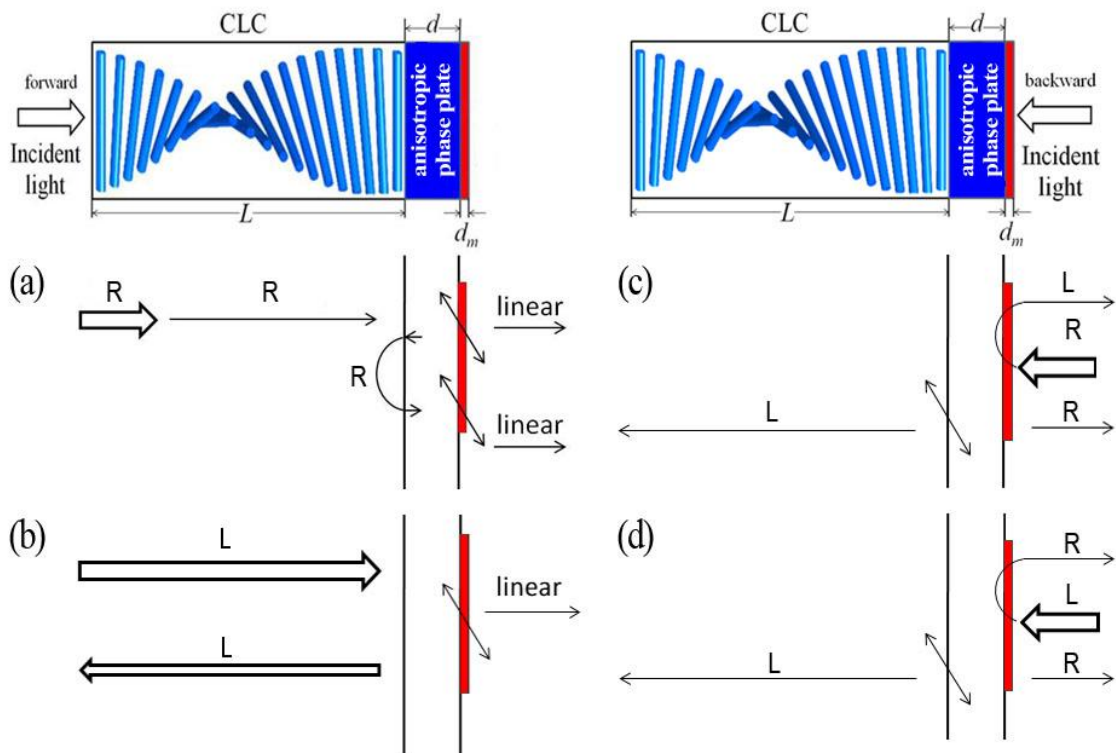


Figure 3.6. Light polarization dynamics at the incidence (a, b) on the CLC and (c, d) on the metal. R and L are the right- and left-hand circular polarization and “linear” is the linear polarization.

When the light falls on the metal (Figure 3.6b), the situation is qualitatively different. It appears that a half of light unabsorbed by the metal and unreflected from it, is reflected from the cholesteric due to the linear polarization.

The situation is similar at the nondiffracting left-hand polarization (Figures 3.6c and 3.6d). Since at the incidence of light on the metal the light of the both circular polarizations propagates similarly, we can expect that the transmittances corresponding to the OTSs for the left- and right-hand polarizations will almost coincide, which was confirmed by the calculations (Figure 3.5).

The structure under study can be used as a polarization optical diode. The advantages of this optical diode are its tunability and manufacturability, since it consists of only three elements.

3.2.3. Controlling the transmission spectrum of the structure

In contrast to calar structures, the transmission spectra of the CLCs can be easily and effectively controlled, because the transmission spectra of the CLCs are different for different polarizations and the helix pitch of the entire CLC or its part can be changed by an external field [84]. The change in the CLC helix pitch will lead to the change in the position of the Bragg reflection region in the crystal.

As was shown in [90], the localized mode is excited in the sample by light of different polarizations, which though make different contributions to the excitation. This effect is explained by the fact that light of the both circular polarizations excites a localized mode by transforming the polarizations at the dielectric interfaces. As a result, any polarization of light becomes elliptic, to different extents, at the CLC output, depending on the initial polarization and crystal thickness. A typical transmission spectrum for right, left and linear polarizations with polarization plane transversely or longitudinally to the orientation of the molecules at the entrance to the cholesteric sample polarizations of light is shown in Figure 3.7.

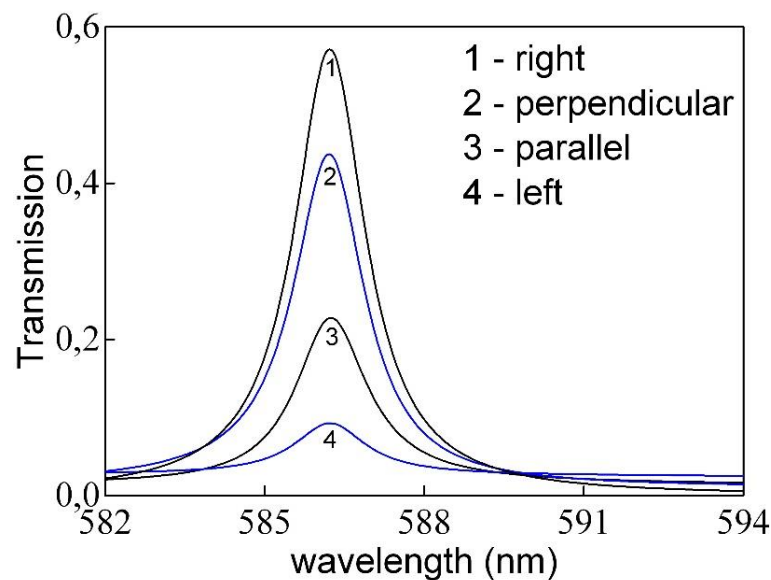


Figure 3.7. Transmission spectrum associated with different polarizations of light tunneling through the localized mode.

We investigated transmission of the linearly polarized light by the structure. It was established that the transmittance of the structure at the frequency corresponding to the OTS depends on angle φ between the optical axis of the phase plate and the polarization plane of polarization of the incident linearly polarized light (Figure 3.8a).

It can be seen from the plots that the transmission maxima at the propagation of light in the forward and backward directions are shifted relative to each other. When the light falls on the metal, the transmittance of the structure is maximum at an angle of 45° between the plane of polarization of the incident light and the optical axis of the phase plate. This is caused by transformation of the linear polarization to the circular one during propagation of light through the quarter-wave phase plate. Consequently, all the light that reaches the CLC will pass through it.

Figure Figure 3.8b shows the dependence of the maximum squared absolute value of the electric field for different angles φ . Using this dependence, one can determine the polarization at which the radiation is the most effectively localized in the system. It can be seen that the localization at the frequency corresponding to the localized state at the light incidence on the CLC multiply exceeds that at the light incidence on the metal film.

By varying parameters of the system we can control position of the transmission peak via an isolated surface waveguide mode. Strong dependence of the helical pitch, e.g. on temperature, as compared to other structural elements, can be used to effectively control frequency of the transmission peak associated with tunneling of light through the surface state.

Figure 3.9.shows the dependence of the electric field intensity on the peak frequency as a function of the CLC helix pitch.

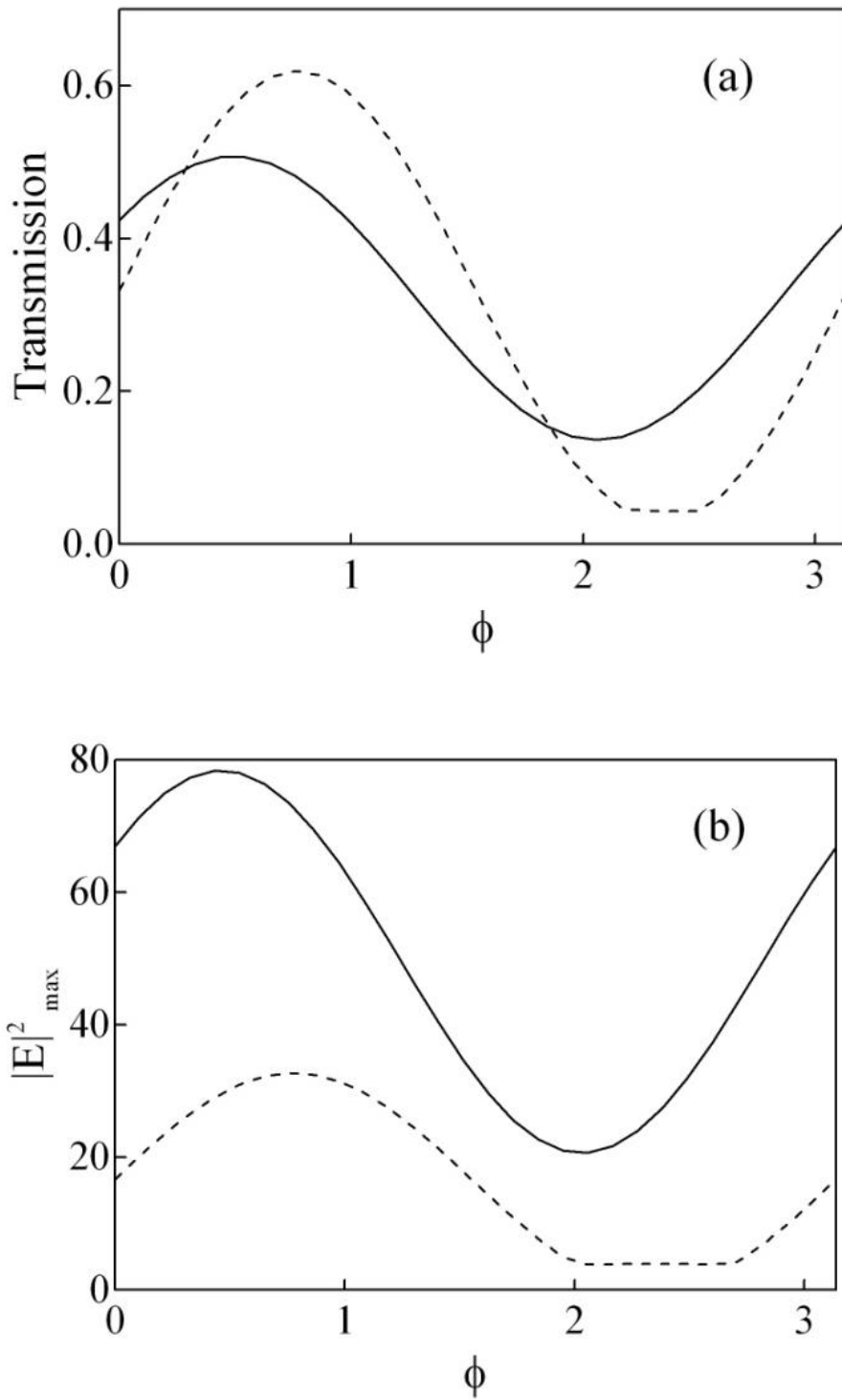


Figure 3.8.(a) Transmittances corresponding to the localized state at different ϕ for the light falling on the CLC (solid line) and on the metal (dashed line). (b) Electric field intensity at the OTS frequency at different ϕ for the light falling on the CLC (solid line) and on the metal (dashed line).

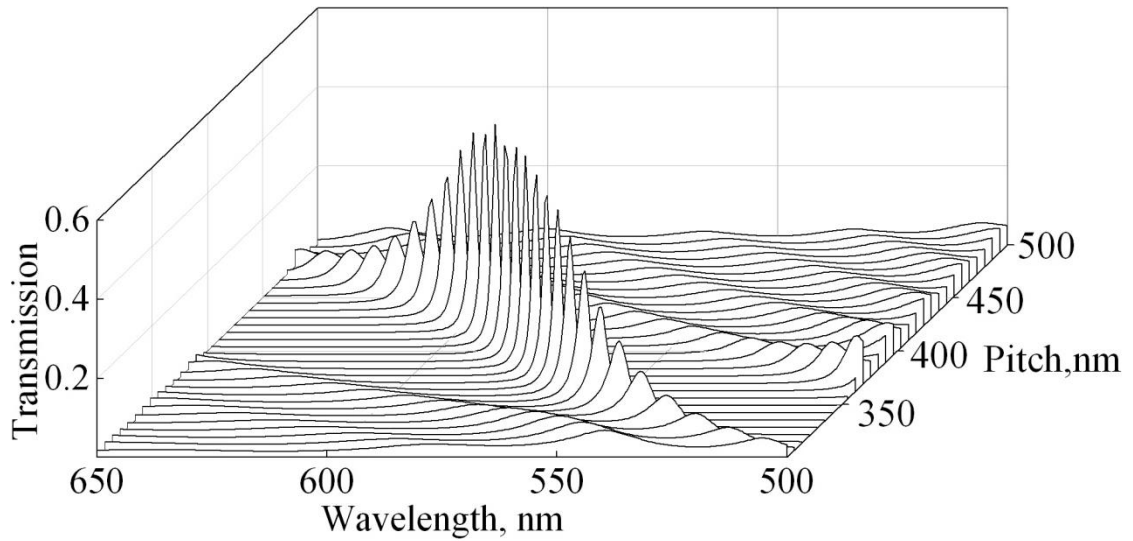


Figure 3.9. Transmission spectrum of the structure versus cholesteric helix pitch.

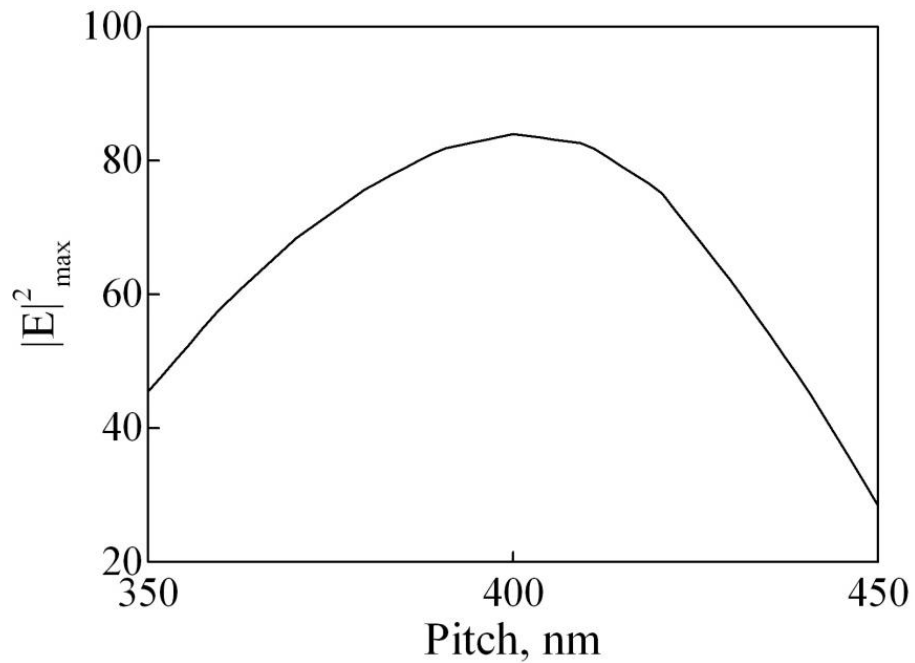


Figure 3.10. The maximum local intensity of the electric field (in units of the incident field intensity) at the localized state frequency, depending on the CLC helix pitch

The maximum intensity of the field for the helix pitch of the CLC is 400 nm, corresponding to a maximum transmission at a wavelength of $\lambda = 586$ nm.

3.3. Localized Optical States in a Structure Formed by Two Oppositely Handed Cholesteric Liquid Crystal Layers and a Metal

In last chapters, we investigated the properties of the structure with a thin CLC layer and a metal film. It was shown that to excite the localized states, the structure should include a quarter-wavelength anisotropic plate inserted between the CLC and metal layer. This is related to the variation in the wave polarization upon reflection from the metal and to the specific polarization properties of the CLCs. The parameters of the phase plate should satisfy the approximate relation (3.1). Thus, the imposed conditions relating the parameters of the phase changing element and CLC are fairly strict.

The aim of this paragraph is to consider another way of implementing the states localized at the CLC/metal interface without using a quarter-wavelength layer. For this purpose, we propose to use one more cholesteric layer with the opposite helix twist, so the resulting system would involve the left-handed cholesteric, right-handed cholesteric, and metal film (Figure 3.11). A few studies of optical properties of CLC structure variants have been published in [26, 91–94].

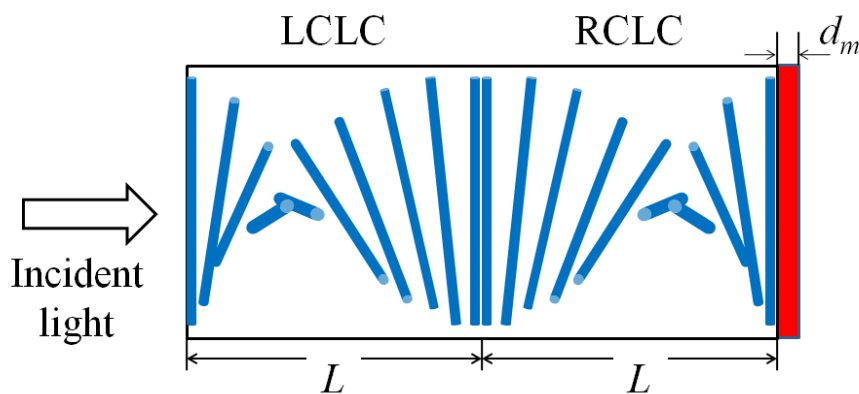


Figure 3.11. Schematic of the structure consisting of two oppositely handed CLCs and a metal layer.

We investigate the properties of the structure consisting of the cholesterics with identical parameters but different helix twist directions. The system is surrounded by a medium with the refractive index equal to the average refractive index of the CLCs. The crystal thicknesses are $L = 2 \mu\text{m}$, the helix pitch is $p = 0.4 \mu\text{m}$, and the ordinary and extraordinary refractive indices are $n_o = 1.4$ and $n_e = 1.6$, respectively. In this case, the stop band lies between 560 and 640 nm. The angle between the directors at the cholesteric interface is α . Here, we consider the light incidence onto the CLC. At the light incidence onto the metal, the results will be analogous. The metal layer was made of silver, for which the real part of the permittivity is negative at the wavelengths of the CLC stop band.

The silver film thickness was $d_m = 50 \text{ nm}$. The metal permittivity was specified in the form of the Drude approximation (2.2) where the constants corresponds the silver.

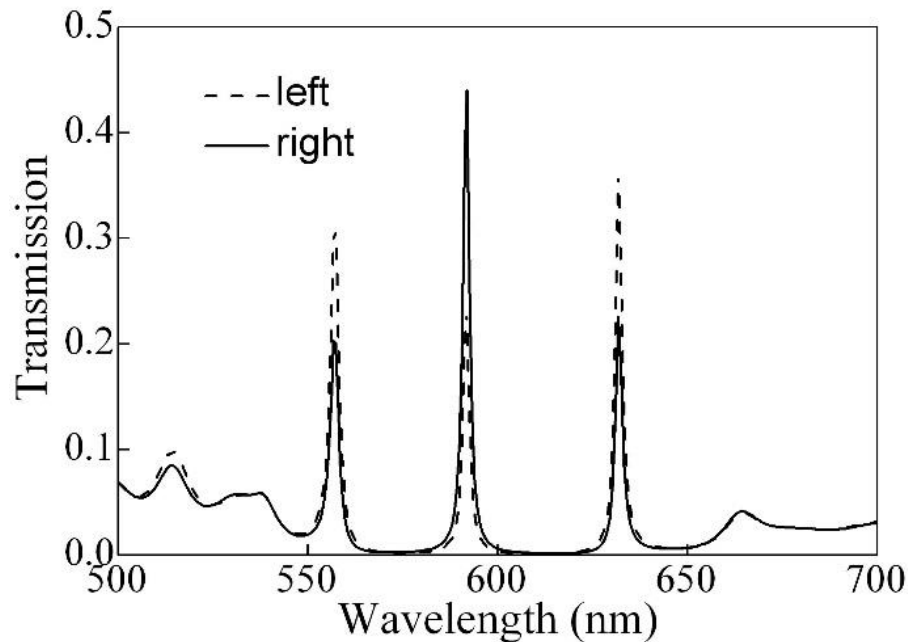


Figure 3.12. Transmission spectrum of the structure for circular polarizations.

Figure 3.12 shows the calculated transmission spectrum for circularly polarized light. At wavelengths of $\lambda = 557, 591,$ and 632 nm, the transmission peaks corresponding to the localized states are observed. As is known, the band gap of a cholesteric depends on its thickness [5]. At $L = 2 \mu\text{m}$, these wavelengths lie in the CLC stop band. The electric field distribution at the wavelengths 591 nm corresponding to the transmission maximum is illustrated in Figure 3.13. The light is localized near the metal film with the maximum electric field value at the CLC/metal interface. Damping of the localized mode field inside the metal is caused by the negative permittivity of the metal film, while damping of this field inside the CLC results from the Bragg reflection.

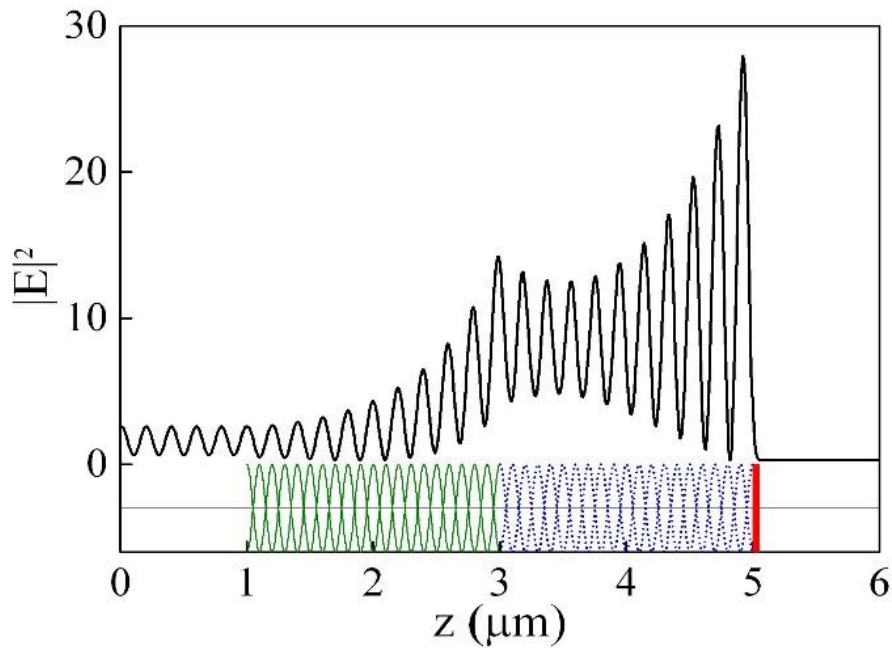


Figure 3.13. Localization of light with the right circular polarization at $\lambda=591$ nm.

The incident light of any polarization is localized with the field intensity maximum at the metal/CLC interface. However, different polarizations of the waves passed through the CLC yield different transmittances.

Varying the angle α between the directors at the cholesteric boundary, one can reconstruct the transmission spectrum of the structure. Depending on α , the

peaks will have different positions in the spectrum (Figure 3.14). The spectra change with a period of 180° by the angle α . We established that at $\alpha = 90^\circ$, the transmission spectra for the right- and left-handed circular polarizations coincide. This means that, although the intrinsic waves for both cholesterics are the quasi-circularly polarized planar waves, the intrinsic waves for the investigated system at $\alpha = 90^\circ$ will be linearly polarized. Therefore, at a certain linear polarization, the transmittance can exceed 0.7.

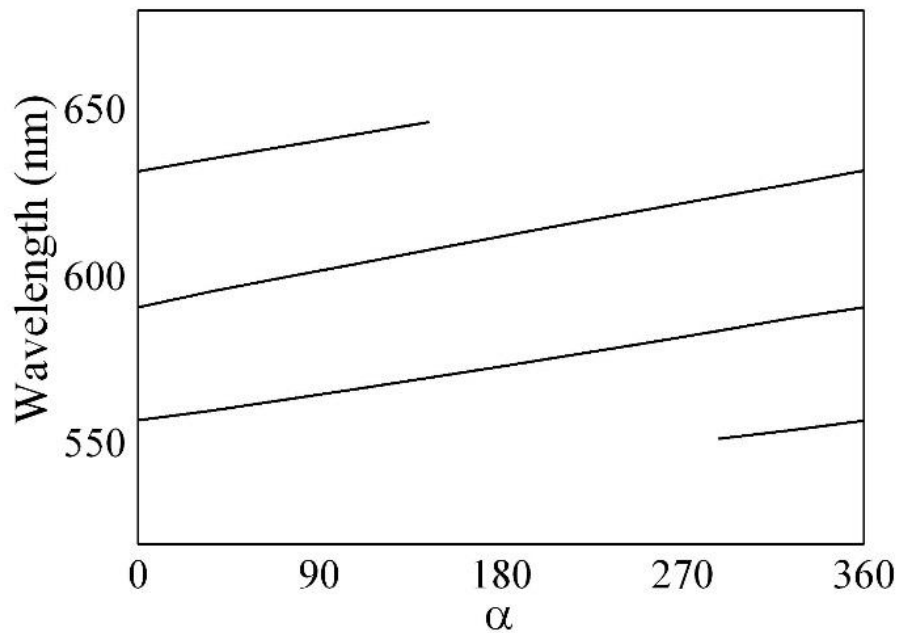


Figure 3.14. The dependence of wavelength for maximum transmission for right circular polarization vs angle α .

The metal film thickness affects not only the transmittance of the structure, but also the degree of light localization between the CLC and metal. The calculated light localization maximum at the localized state frequency for the cases of light incidence onto the CLC and metal is presented in Figure 3.15. It can be seen that there is the maximum degree of light localization that remains almost invariable with a further increase in the metal layer thickness. This originates from the fact that as the metal thickness is further increased, the light absorption stays nearly constant; consequently, the reflection also remains the

same. When the light is incident onto the metal film, the investigated dependence behaves differently: the degree of localization reaches its minimum and then does not change. This is due to the fact that the larger part of radiation is absorbed at the input to the system. Therefore, the light is localized stronger when it falls from the CLC side.

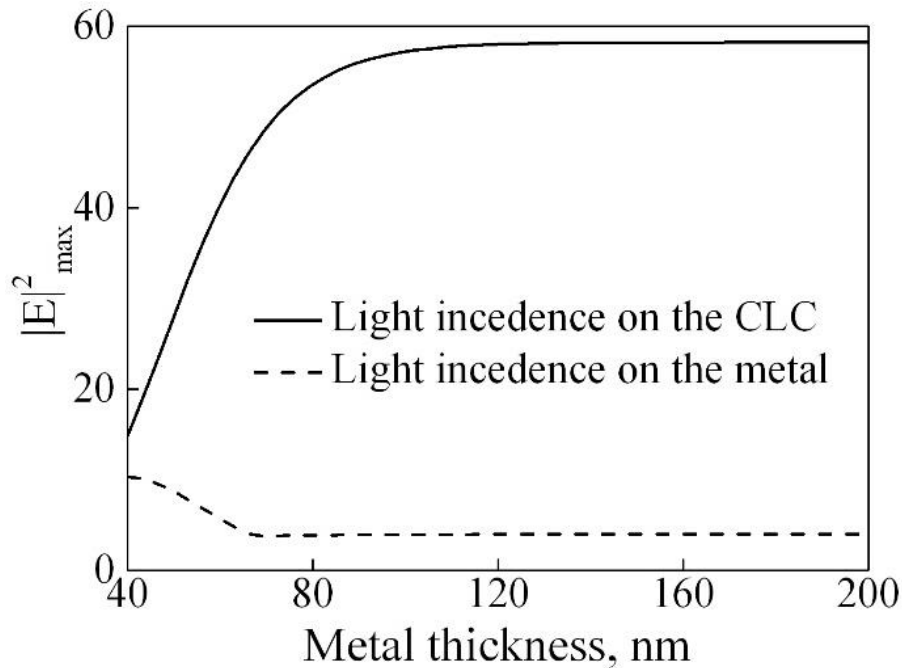


Figure 3.15. Electric field intensity for maximal localization wavelength vs metal thickness at the light incidence onto the CLC and the metal.

An increase in the CLC layer thickness leads to an increase in the number of spectral peaks (Figure 3.16). The simulation showed that the spectrum is extremely sensitive to the wave phase variation during propagation along the structure and to the reflection from the structural elements. The localized states occur only when the thickness of the oppositely handed CLCs are almost the same.

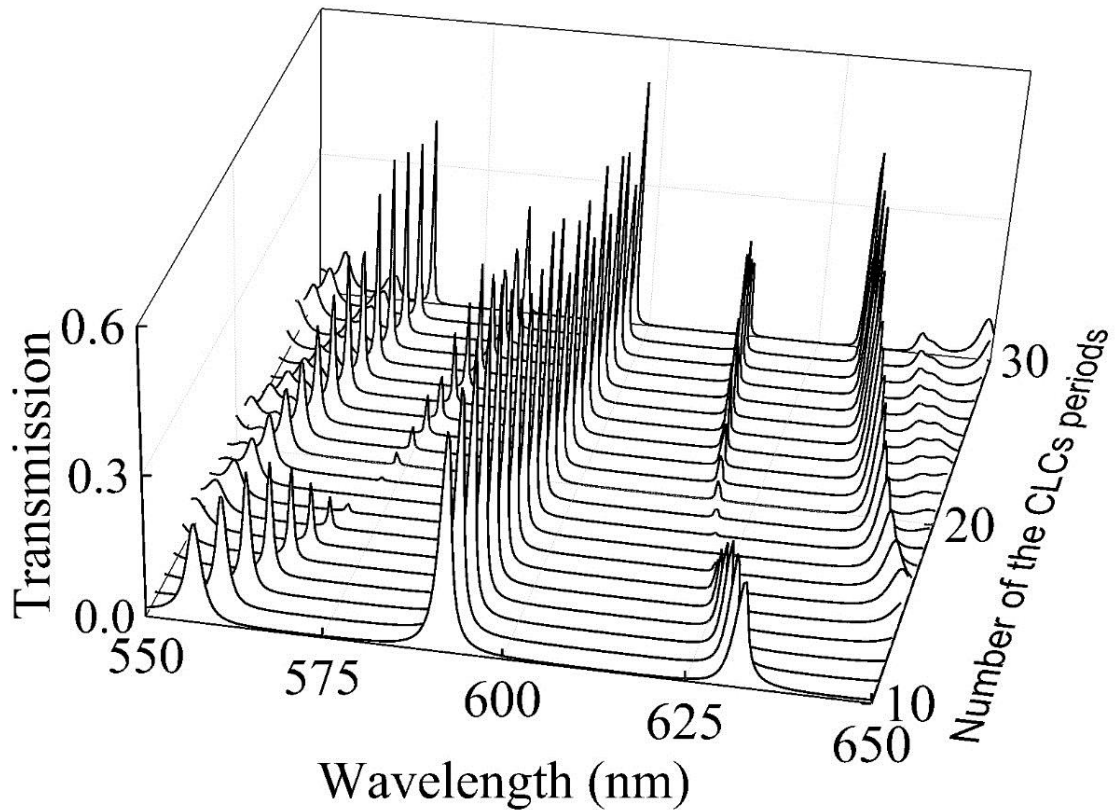


Figure 3.16. The dependence of transmission spectrum for the right-handed circular polarization on period number of the two CLCs; $\alpha = 0$.

Moreover, we should discuss the possibility of experimental implementation of the investigated structure. The simplest way of forming a contact between two CLCs is to use polymer CLCs, as was made in [26].

We should fabricate two polymer CLC films with different helix twists, but the same helix pitch and refractive index (Figure 3.17). For this purpose, one substrate is coated with an orienting layer, e.g., a rubbed polyimide film coated with the polymer CLC layer. The other substrate is coated first with the metal, then with the orienting layer, and, finally, with the polymer CLC layer. The substrates with the deposited layers are connected using an immersion liquid to make an optical contact between the cholesteric films. The angle α between the directors at the cholesteric boundary interface is specified by the angle between the rubbing directions of the orienting polyimide films. Instead of polyimide, it is possible to use photo-orientation [95].

We studied the effect of the rubbed polyimide film [96] (thickness 100 nm, refractive index 1.6) and immersion liquid on the spectral properties of the structure and established that the localized states arise with disregard of the layer thicknesses, but their number directly depends on the thicknesses of structure elements. The thickness of the immersion liquid layer between two CLCs affects the spectral properties of the structure stronger than the thickness of the layer between the metal and orienting cholesteric.

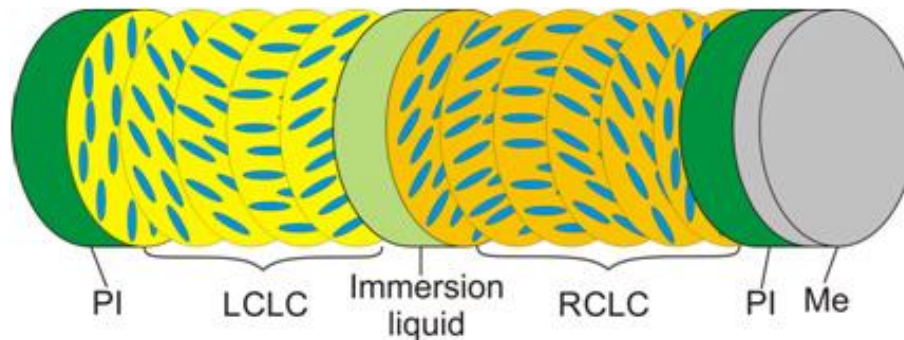


Figure 3.17. Schematic of the experimental structure

In addition, we would like to mention one potential application of the discussed states. Zhang et. al. [97] showed that the broadband absorption of organic solar cells can be enhanced via excitation of the OTSs. Rodarteet. al. [98] lately proposed a photonic cholesteric luminescent solar concentrator doped with a dye. In our opinion, these two ideas can be united by combining the CLC and localized optical states predicted in this work.

3.4. Localized Optical States in a Liquid-Crystal Structure Adjacent to a Metal

Some authors [26,27,32,99-100] have studied CLC systems with an anisotropic defect layer. The authors of [100] designed optical CLC cells with electrodes formed perpendicular to the CLC helix axis. Using such cells, they managed to untwist the CLC helix in the middle of the layer and, thereby, form a planar defect. Hsiao et al. [32] used the thermodielectric effect to induce a local strain at the center of a one-dimensional periodic helical structure.

Based on these studies, we investigated a structure consisting of a metallic film and a CLC with the planar defect (Figure 3.18). The CLC-layer thickness was $L = 11 \mu\text{m}$, the helix pitch was $p = 0.4 \mu\text{m}$, and the ordinary and extraordinary refractive indices were $n_o = 1.45$ and $n_e = 1.55$, respectively. At these parameters, the CLC band gap lies between 580 and 620 nm. In the middle of the layer, the CLC helix is untwisted at a length of $3 \mu\text{m}$, which is analogous to a quarter-wave anisotropic defect positioned there. The structure is surrounded by a medium with the refractive index equal to the averaged CLC refractive index. The thickness of the metallic film was $d_m = 50 \text{ nm}$, and its permittivity was specified by the Drude approximation (2.2).

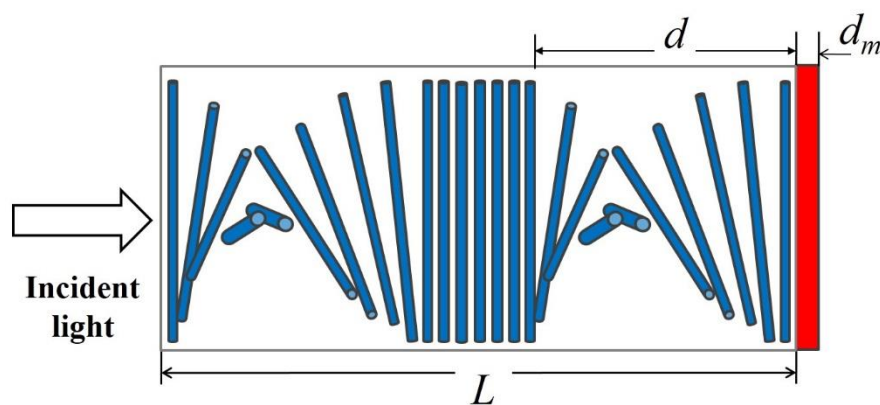


Figure 3.18. Schematic of the investigated structure.

As was demonstrated in [27, 99], the presence of a half-wave defect layer in the CLC structure leads to the loss of the polarization dependence of the diffraction reflection. It means that the CLC starts reflecting light of any polarization rather than only the circularly polarized radiation with the direction coinciding with the CLC helix twist. Figure 3.19 shows the calculated transmission spectrum of the circularly polarized light for the investigated system CLC–half-wave defect–CLC–metal. At the frequencies of the Bragg reflection zone in the crystal, several transmission peaks occurred. Note that these peaks are observed at both circular polarizations.

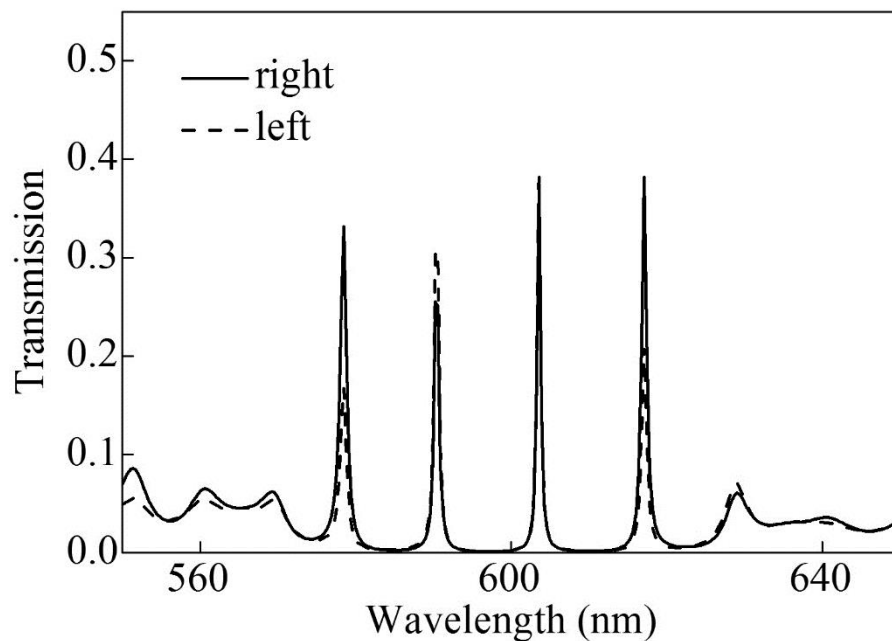


Figure 3.19 Transmission spectrum of the structure for circularly polarized incident light.

Each peak in the spectrum corresponds to the localized state. Figure 3.20 shows the electric-field intensity distribution for the right-hand circular polarization at a wavelength of 603.5 nm. At the rest of the frequencies, the field distribution is analogous. The field is mainly localized at the metal-CLC interface. The localized-mode field attenuation inside the metal is caused by the negative permittivity of the metallic film, whereas the field attenuation inside the

CLC results from the Bragg reflection. Note that the field is partially localized on the defect with the maximum in the middle of the half-wave layer. This is due to the fact that the system under study can be considered as a composition of several resonators. The planar defect can be considered as one of them.

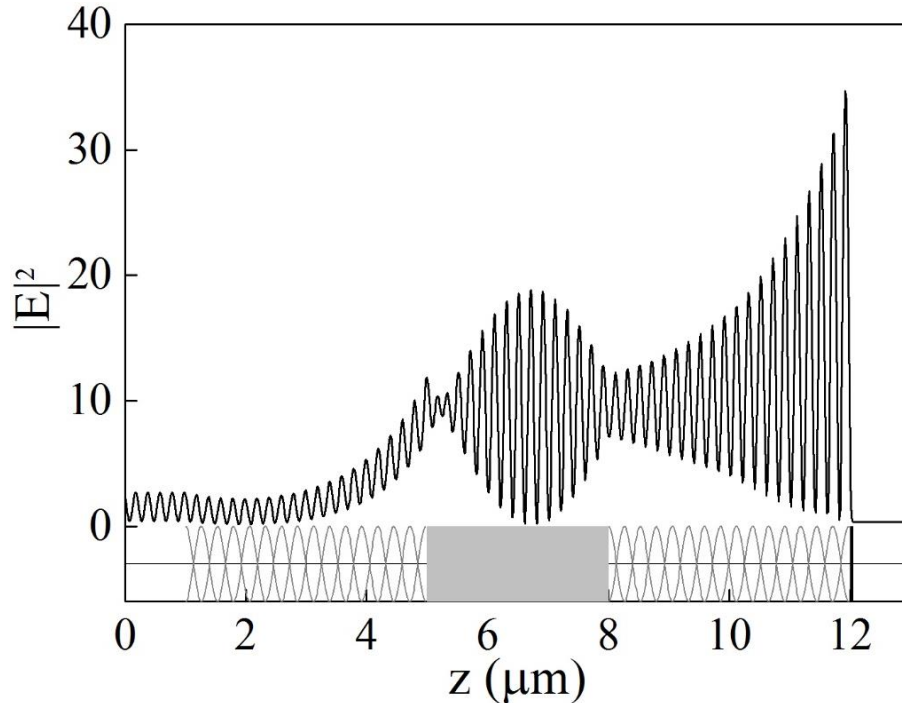


Figure 3.20. Electric-field-intensity distribution for right-hand circular polarization of the incident light at a wavelength of 603.5 nm.

Let us investigate the variation in the properties of the structure with the planar defect position in the CLC. The calculated transmission spectrum at different positions of the defect relative to the CLC center is shown in Figure 3.21. It can be seen that the transmission spectrum significantly depends on the defect position in the CLC. As the distance between the defect and metal decreases, the resonances gradually vanish. As the distance increases, the peaks move closer to each other and the transmission at their frequencies grows. This originates from the fact that the reflectance of the CLC layer depends on its thickness. At small CLC layer thicknesses, the majority of the light between the metal and defect passes through this layer, changes its orientation when passing through the half-

wave defect, and exits from the second CLC layer. Thus, the light localization is affected mainly by the CLC part located between the defect and metallic film.

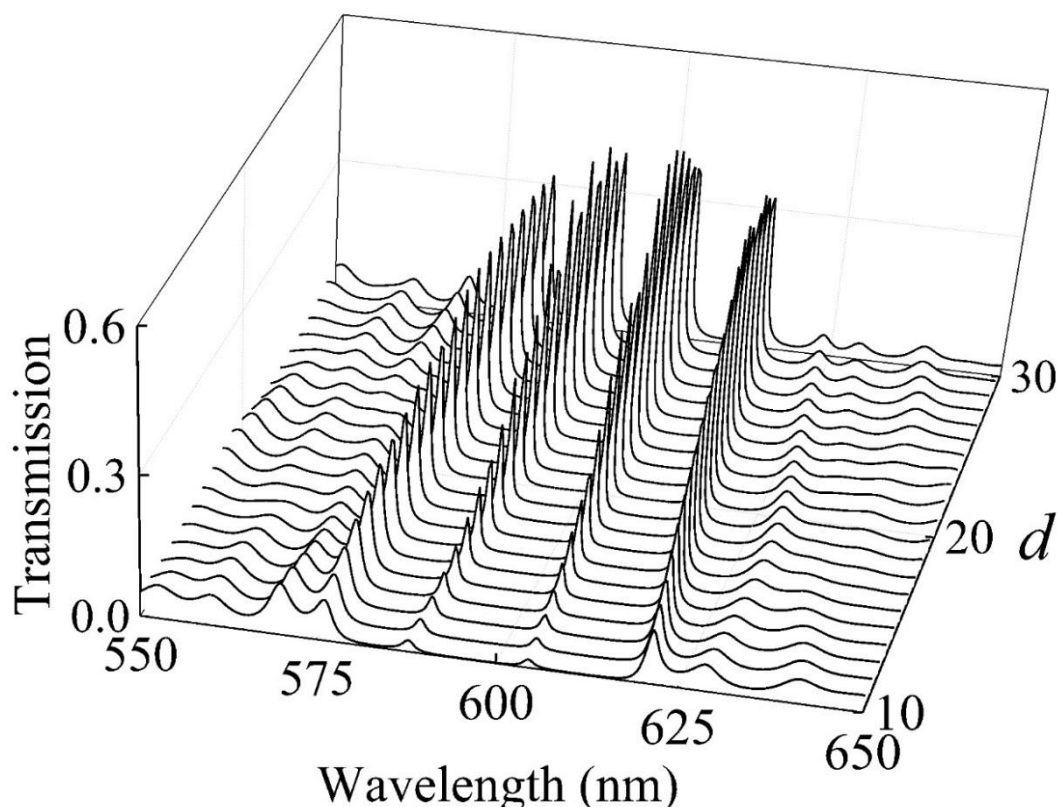


Figure 3.21. Dependence of the transmission spectrum for right-hand circular polarization on number of periods d between the defect and metal.

Thus, we demonstrated the existence of surface electromagnetic states localized in the structure containing a silver film and CLC with a half-wave planar defect. This defect can be induced, e.g., by applying an external electric field perpendicular to the CLC helix axis. It was established that at this geometry the light with any polarization of the incident wave is localized with the maximum field intensity at the metal–CLC interface. Different ellipticities of the waves passing through the CLC and their polarization properties lead to different transmittances for each polarization. It was shown that the transmission spectrum of the investigated structure significantly depends on the defect position in the CLC.

SUMMARY

Using the numerical analysis of spectral properties, defect and localized modes of photonic crystal structures based on cholesteric liquid crystals are investigated.

We studied defect modes of a cholesteric liquid crystal with a resonant absorbing defect layer of nanocomposite combined with a phase jump of cholesteric helix at the interface between nanocomposite and cholesteric layers. We have studied the manifestation of the effect of splitting of defect modes induced for incident light in the transmission spectra. We have shown that it is possible to effectively control the transmission spectrum of CLC with a combined defect by varying the angle of incidence of light on the CLC or by applying external fields to vary the helix pitch. There are such angles of incidence or helix pitches that the NC resonant frequency appears to be close to the boundary of the CLC band gap, which facilitates the emergence of an extra transmission band for waves of both circular polarizations of incidence light. New spectral features arise when the CLC helix pitch is modified on just one side from the defect layer. Increasing the helix pitch leads to widening of photonic band gap of the structure and repositioning of the defect modes. It has been revealed that the electric field maximum of the localized mode varies nonmonotonously with the helix pitch p_2 .

We demonstrated the existence of surface electromagnetic states localized in ‘cholesteric liquid crystal–phase plate–metal’ structure. It was shown that the system could have an isolated waveguide surface mode with characteristics efficiently controllable by external fields acting on the cholesteric. The degree of localization of surface modes and the transmission coefficients have been found to differ considerably for the light of different polarizations. Light of any polarization will be localized near metal with the field intensity maximizing at the phase plate – metal layer interface. However, different degrees of ellipticity of transmitted waves and their polarization properties resulted in different

transmission coefficients for each polarization. We showed that the transmission spectra for the light propagating in the forward and backward direction were different; i.e., we dealt with the transmission anisotropy. Therefore, the investigated structure can be used as a polarization optical diode based on surface photonic modes.

We demonstrated the existence of the surface states localized in the structure containing a silver layer and two identical cholesteric liquid crystals with the opposite twist directions. We showed the possibility of controlling the transmission spectrum of the system by varying the angle α between the directors at the boundary interface of the oppositely handed cholesterics. It was established that the dependence of the field localization degree at the localized state frequency on the metal layer thickness behaved differently at different light propagation directions (incidence onto the CLC or metal). As the CLC layer thickness was increased, the number of peaks increased. The possibility of experimental implementation of the proposed structure was discussed.

We demonstrated the existence of surface electromagnetic states localized in the structure containing a silver film and CLC with a half-wave planar defect. This defect can be induced, e.g., by applying an external electric field perpendicular to the CLC helix axis. It was established that at this geometry the light with any polarization of the incident wave was localized with the maximum field intensity at the metal–CLC interface. It was shown that the transmission spectrum of the investigated structure significantly depended on the defect position in the CLC.

REFERENCES

- 1 Photonic Crystals: Molding the Flow of Light / J.D. Joannopoulos [et al.]. – Princeton: Princeton University Press, 2008. – 286 p.
- 2 Sakoda, K. Optical properties of photonic crystals / K. Sakoda. – Berlin: Springer, 2004. – 253 p.
- 3 V. F. Shabanov, S. Ya. Vetrov, and A. V. Shabanov, Optics of Real Photonic Crystals: Liquid Crystal Defects, Irregularities (SB RAS Publisher: Novosibirsk [in Russian], 2005).
- 4 Yariv A., Yeh P. Optical waves in crystals. – Wiley, New York, 1984.
- 5 V. A. Belyakov, Diffraction Optics of Complex Structured Periodic Media, (Springer Verlag, New York, 1992).
- 6 L. M. Blinov, Structure and Properties of Liquid Crystals (Springer, 2011).
- 7 Oseen C. W. The theory of liquid crystals //Transactions of the Faraday Society. – 1933. – V. 29. – P. 883–899.
- 8 deVries H. Rotatory power and other optical properties of certain liquid crystals //ActaCrystallographica. – 1951. – V. 4. – P. 219–226.
- 9 Kats E. I. Optical properties of cholesteric liquid crystals //Sov. Phys. JETP. – 1971. – V. 32. – P. 1004–1007.
- 10 Nityananda, R. On the theory of light propagation in cholesteric liquid crystals //Molecular Crystals and Liquid Crystals. – 1973. – V. 21. – P. 315–331.
- 11 Teitler, S. Refraction in stratified, anisotropic media / S.Teitler, B. W.Henvis//JOSA. – 1970. – V. 60. – P. 830-834.
- 12 Berreman, D.W. Bragg reflection of light from single-domain cholesteric liquid-crystal films / Berreman D. W., Scheffer T. J. //Physical Review Letters. – 1970. – V. 25. – P. 577.
- 13 Abelès F. VI methods for determining optical parameters of thin films //Progress in optics. – 1963. – V. 2. – P. 249–288.

- 14 Jones, R. C. A new calculus for the treatment of optical systems. description and discussion of the calculus //JOSA. – 1941. – V. 31. – P. 488–493.
- 15 Berreman, D.W. Optics in Stratified and Anisotropic Media: 4 X 4-Matrix Formulation / D.W. Berreman // J. Opt. Soc. Am. – 1972. – № 62. – P. 502–510.
- 16 Azzam R M A, Bashara N. M. Ellipsometry and polarized light. North-Holland personal library. North-Holland Pub. Co., 1977.
- 17 Palto, S. P. An algorithm for solving the optical problem for stratified anisotropic media //J. Exp.Theor. Phys. – 2001. – V. 92. – P. 552-560.
- 18 Hodkinson, I. J. Supermodes of Chiral Photonic Filters with Combined Twist and Layer Defects / I. J. Hodkinson, Q. H. Wu, L. De Silva, A. Matthew // Phys. Rev. Lett. – V. 91. – 2003. – P. 223903.
- 19 Hwang, J. Electro-tunable optical diode based on photonic bandgap liquid-crystal heterojunctions / J. Hwang, M.- H. Song, B. Park, S. Nishimura, T. Toyooka, J. W. Wu, Y. Takanishi, K. Ishikawa, H. Takezoe // Nature Materials. – 2005. – V. 4. – P. 383–387.
- 20 Safrani, A. Liquid-crystal polarization rotator and a tunable polarizer / A. Safrani, I. Abdulhalim // Opt. Lett. 2009. – V. 34. – P. 1801–1803.
- 21 A. H. Gevorgyan, M. Z. Harutyunyan, K. B. Oganesyanyan, M. S. Rafayelyan, Optics 123, 2076 (2012).
- 22 Coles, H. Liquid-crystal lasers / H. Coles and S. Morris //Nature Photonics. – 2010. – V. 4. – P. 676–685.
- 23 I. P. Il'chishin, E. A. Tikhonov, V. G. Tishchenko, and M.T. Shpak, JETP Lett. 32, 24 (1980).
- 24 Jeong, S. M. Defect mode lasing from a double-layered dye-doped polymeric cholesteric liquid crystal films with a thin rubbed defect layer/ S. M. Jeong, N. Y. Ha, Y. Takanishi, K. Ishikawa, H. Takezoe, S. Nishimura, G. Suzuki // Appl. Phys. Lett. – 2007. – V. 90. – P. 261108.

- 25 Yang, Y.-C. Photonic defect modes of cholesteric liquid crystals / Y.-C. Yang, Kee C.-S., Kim J.-E. H.Y. Park, J.C. Lee // *Phys.Rev.E.* – 1999. – V. 60, № 6. – P. 6852–6854.
- 26 Song, M. H. Effect of Phase Retardation on Defect-Mode Lasing in Polymeric Cholesteric Liquid Crystals / M. H. Song, B. Park, K. C. Shin, T. Ohta, Y. Tsunoda, H. Hoshi, Y. Takanishi , K. Ishikawa , J. Watanabe , S. Nishimura , T. Toyooka , Z. Zhu, T.M. Swager , H. Takezoe// *Adv. Mat.* – 2004. – V.16. – P. 779–783.
- 27 Gevorgyan, A. H. Chiral photonic crystals with an anisotropic defect layer / A. H. Gevorgyan, M. Z. Haratyunyan. // *Phys. Rev. E* – 2007. – V. 76. – P. 031701.
- 28 Hodkinson, I. J. Spacerless circular-polarization spectral-hole filters using chiral sculptured thin films: theory and experiment / I. J. Hodkinson, Q. H. Wu, K. E. Thorn, A. Lakhtakia, M. W. McCall // *Opt. Comm.* – 2000. V. 184. – P. 57–64.
- 29 Kopp, V. I. Twist Defect in Chiral Photonic Structures / V. I. Kopp, A. Z. Genack. // *Phys. Rev. Lett.* – 2002. – V. 89. – P. 033901.
- 30 Shabanov, A. V. Reflection spectrum of a cholesteric liquid crystal with structural defects / A. V. Shabanov, S. Y. Vetrov, A. Y. Karneev// *JETP Letters.* – 2004. – V. 80. – P. 181–184.
- 31 Matsui, T. Tunable photonic defect modes in a cholesteric liquid crystal induced by optical deformation of helix / T. Matsui, M. Ozaki, K. Yoshino. // *Phys. Rev. E.* – 2004. – V. 69. – P. 061715.
- 32 Hsiao, Y.-C. Thermodielectric generation of defect modes in a photonic liquid crystal / Y.-C. Hsiao, H.-T. Wang, W. Lee // *Opt. Exp.* – 2014. – V. 22. – P. 3593–3599.
- 33 Belyakov, V. A. Optical defect modes in chiral liquid crystals / V. A. Belyakov, S. V. Semenov // *J. Exp.Theor. Phys.* – 2011. – T. 112. – P.694-710.

- 34 Becchi, M. Defect modes in helical photonic crystals: An analytic approach / M. Becchi, S. Ponti, J. A. Reyes, C. Oldano. // *Phys. Rev. B*. 2004. – V. 70. – P. 033103.
- 35 Wang, F. Specular and nonspecular, thickness-dependent, spectral holes in a slanted chiral sculptured thin film/ F. Wang, A. Lakhtakia // *Opt. Comm.* – 2003. – V. 215. – P. 79–92.
- 36 Schmidtke, J. W. Defect Mode Emission of a Dye Doped Cholesteric Polymer Network / J. Schmidtke, W. Stille // *Eur. Phys. J. E.* – 2003. – V. 12. – P. 553–562.
- 37 Oraevskii, A. N. High refractive index and other optical properties of heterogeneous media / A. N. Oraevskii, I. E. Protsenko // *JETP Letters.* – 2000. – V. 72. – P. 445–448.
- 38 Oraevskii, A. N. Optical properties of heterogeneous media / A. N. Oraevskii, I. E. Protsenko // *Quant. Elect.* – 2001. – V. 31. – P. 252.
- 39 Moiseev, S. G. Nanocomposite-Based Ultrathin Polarization Beamsplitter / S. G. Moiseev // *Opt. and Spectr.* – 2011. – V. 111. – P. 233–243.
- 40 Pedrueza, E. Novel Method of Preparation of Gold-Nanoparticle-Doped TiO₂ and SiO₂ Plasmonic Thin Films: Optical Characterization and Comparison with Maxwell–Garnett Modeling/ E. Pedrueza J. L. Valdes, V. Chirvony, R. Abargues, J. Hernandez-Saz, M. Herrera, S. I. Molina, J. P. Martinez-Pastor // *Adv. Funct. Mater.* – 2011. – V. 21. – P. 3502–3507.
- 41 Vetrov, S. Ya. Spectral properties of a one-dimensional photonic crystal with a resonant defect nanocomposite layer / S. Ya. Vetrov, A. Y. Avdeeva, I. V. Timofeev // *J. Exp. Theor. Phys.* – 2011. – V. 113. – P. 755–761.
- 42 Moiseev, S. G. Defect mode suppression in a photonic crystal structure with a resonance nanocomposite layer / S. G. Moiseev, V. A. Ostatochnikov, D. I. Sementsov // *Quant. Elect.* – 2012. – V. 42. – P. 557.

- 43 Vetrov, S. Ya. Specific Features of the Spectral Properties of a Cholesteric Liquid Crystal with a Resonance Defective Nanocomposite Layer / S. Ya. Vetrov, M. V. Pyatnov, I. V. Timofeev // *Physics of the Solid State*. – 2013. – V. 55. – P. 1697–1702.
- 44 Vetrov, S. Ya. Photonic defect modes in a cholesteric liquid crystal with a resonant nanocomposite layer and a twist defect / S. Ya. Vetrov, M. V. Pyatnov, I. V. Timofeev // *Phys. Rev. E*. – 2014. – V. 90. – P. 032505.
- 45 Moiseev, S. G. Defect modes of one-dimensional photonic-crystal structure with a resonance nanocomposite layer / S. G. Moiseev, V. A. Ostatochnikov // *Quant. Elect.* – 2016. – V. 46. – P. 743–748.
- 46 Garnett Maxwell J. C. Colours in metal glasses, in metallic films, and in metallic solutions. II / J. C. Maxwell Garnett // *Philosophical Transactions of the Royal Society of London. Series A, Containing Papers of a Mathematical or Physical Character*. – 1906. – P. 237–288.
- 47 Golovan, L. A. Optical properties of porous-system-based nanocomposites / L. A. Golovan, V. Yu. Timoshenko, P. K. Kashkarov. // *Phys. Usp.* – 2007. – V. 50. – P. 595–612.
- 48 Johnson, P. B. Optical constants of the noble metals / P. B. Johnson, R. W. Christy // *Phys. Rev. B*. – 1972. – V. 6. – P. 4370–4379.
- 49 Timofeev, I. V. Voltage-induced defect mode coupling in a one-dimensional photonic crystal with a twisted-nematic defect layer / I. V. Timofeev, Y.-T. Lin, V. A. Gunyakov, S. A. Myslivets, V. G. Arkhipkin, S. Y. Vetrov, W. Lee, V. Y. Zyryanov // *Physical Review E*. – 2012. – V. 85. – P. 011705.
- 50 Wang, H.-T. Tunable narrow-bandpass filter based on an asymmetric photonic bandgap structure with a dual-mode liquid crystal / H.-T. Wang, I. V. Timofeev, K. Chang, V. Ya. Zyryanov, W. Lee // *Opt. Exp.* – 2014. – V. 22. – P. 15097.

- 51 Vinogradov, A. P. Surface states in photonic crystals / A. P. Vinogradov, A. V. Dorofeenko, A. M. Merzlikin, A. A. Lisyansky // *Phys. Usp.* – 2010. – V. 53.– P. 243–256.
- 52 Kavokin, A. Optical Tamm states for the fabrication of polariton lasers / A. Kavokin, I. Shelykh, and G. Malpuech // *Appl. Phys. Lett.* – 2005. – V. 87. – P. 261105.
- 53 Kavokin, A. V. Lossless interface modes at the boundary between two periodic dielectric structures / A. V. Kavokin, I. A. Shelykh, G. Malpuech // *Phys. Rev. B.*– 2005. – V. 72.– P. 233102.
- 54 Kaliteevski, M. Tamm plasmon-polaritons: Possible electromagnetic states at the interface of a metal and a dielectric Bragg mirror / M. Kaliteevski, I. Iorsh, S. Brand, R. A. Abram, J. M. Chamberlain, A. V. Kavokin, I. A. Shelykh // *Phys. Rev. B.* – 2007. – V. 76. – P. 165415
- 55 Vetrov, S. Ya. The optical Tamm states at the edges of a photonic crystal bounded by one or two layers of a strongly anisotropic nanocomposite/ S. Ya. Vetrov, R. G. Bikbaev, I. V. Timofeev // *Opt. Comm.* – 2017. – V. 395.– P. 275–281.
- 56 Núñez-Sánchez, S. Excitonic Optical Tamm States: A Step toward a Full Molecular–Dielectric Photonic Integration /S. Núñez-Sánchez, M. Lopez-Garcia, M. M. Murshidy, A. G. Abdel-Hady, M. Serry, A. M. Adawi, J. G. Rarity, R. Oulton, W. L. Barnes // *ACS Photon.* – 2016. – V. 3. –P. 743-748.
- 57 Sasin, M. E. Tamm plasmonpolaritons: Slow and spatially compact light / M. E. Sasin, R. P. Seisyan, M. A. Kalitseevski, S. Brand, R. A. Abram, J. M. Chamberlain, A. Yu. Egorov, A. P. Vasil'ev, V. S. Mikhrin, A. V. Kavokin // *Appl. Phys. Lett.* – 2008. V. 92. – P. 251112.
- 58 Goto, T. / Optical Tamm States in One-Dimensional Magnetophotonic Structures / T. Goto, A. V. Dorofeenko, A. M. Merzlikin, A. V. Baryshev, A. P. Vinogradov, M. Inoue, A. A. Lisyansky, A. B. Granovsky // *Phys. Rev. Lett.* – 2008. – V. 101. – P. 113902.

- 59 Huang, S.-G. Phase sensitive sensor on Tamm plasmon devices / S.-G. Huang, K.-P. Chen, S.-C. Jeng // *Opt. Mater. Exp.* – 2017. – V. 7. –P. 1267-1273.
- 60 Auguie, B. Tamm plasmon resonance in mesoporous multilayers: toward a sensing application / B. Auguie, M. C. Fuertes, P. C. Angelomé, N. L. Abdala, G. J. A. A. Soler Illia, and A. Fainstein / *ACS Photon.* – 2014. – V. 1. –P. 775–780.
- 61 Zhang, W. L. Bistable switching using an optical Tamm cavity with a Kerr medium / W. L. Zhang, S. F. Yu. // *Opt. Commun.* – 2010. – V. 283. – P. 2622-2626.
- 62 Kwang, J. L. Enhanced nonlinear optical effects due to the excitation of optical Tamm plasmon polaritons in one-dimensional photonic crystal structures / J. L. Kwang, J. W. Wu, K. Kim // *Opt. Express.* – 2013. – V. 21. – P. 28817–28823.
- 63 Vinogradov, A. P. Surface state peculiarities in one-dimensional photonic crystal interfaces / A. P. Vinogradov, A. V. Dorofeenko, S. G. Erokhin, M. Inoue, A. A. Lisyansky, A. M. Merzlikin, A. B. Granovsky – *Phys. Rev. B.* – 2006. – V. 74. – P. 045128.
- 64 Zhang, X.-L. Optical Tamm states enhanced broad-band absorption of organic solar cells / X.-L. Zhang, J.-F. Song, X.-B. Li, J. Feng, H.-B. Sun // *Appl. Phys. Lett.* – 2012. – V. 101. –P. 243901.
- 65 Zhang, X.-L. Light trapping schemes in organic solar cells: A comparison between optical Tamm states and Fabry–Pérot cavity modes / X.-L. Zhang, J.-F. Song, X.-B. Li, J. Feng, H.-B. Sun // *Organic Electronics.* – 2013. – V. 14. – P. 1577-1585.
- 66 Yang, F. Visibly transparent organic photovoltaic with improved transparency and absorption based on tandem photonic crystal for greenhouse application / F. Yang, Y. Zhang, Y. Hao, Y. Cui, W. Wang, T. Ji, F. Shi, B. Wei, // *Applied optics.* – 2015. – V. 54. – P. 10232–10239.

- 67 Gong, Y. Perfect absorber supported by optical Tamm states in plasmonic waveguide / X. Liu, H. Lu, L. Wang, G. Wang // *Opt. Exp.* – 2011. – V. 19. – P. 18393–18398.
- 68 Zhang, X.-L. Hybrid Tamm plasmon-polariton/microcavity modes for white top-emitting organic light-emitting devices / X.-L. Zhang, J. Feng, X.-C. Han, Y.-F. Liu, Q.-D. Chen, J.-F. Song, H.-B. Sun // *Optica.* – 2015. – V. 2. – P. 579–584.
- 69 Symonds, C. Confined Tamm Plasmon Lasers / C. Symonds, G. Lheureux, J. P. Hugonin, J. J. Greffet, J. Laverdant, G. Brucoli, A. Lemaitre, P. Senellart, J. Bellessa // *Nano. Lett.* – 2013. – V. 13. – P. 3179–3184.
- 70 Lheureux, G. Polarization-controlled confined Tamm plasmon lasers / G. Lheureux, S. Azzini, C. Symonds, P. Senellart, A. Lemaître, C. Sauvan, J. P. Hugonin, J. J. Greffet, J. Bellessa // *ACS photon.* – 2015. – V. 2. – P. 842–848.
- 71 Gazzano, O. Single photon source using confined Tamm plasmon modes / O. Gazzano, S. Michaelis de Vasconcellos, K. Gauthron, C. Symonds, P. Voisin, J. Bellessa, A. Lemaître, P. Senellart // *Appl. Phys. Lett.* – 2012. V. 100. – P. 232111.
- 72 Dong, H. Y. One-way Tamm plasmon polaritons at the interface between magnetophotonic crystals and conducting metal oxides / H. Y. Dong, J. Wang, T. J. Cui // *Phys. Rev. B.* – 2013. – V. 87. – P. 045406.
- 73 Da, H. Monolayer graphene photonic metastructures: Giant Faraday rotation and nearly perfect transmission / H. Da, Q. Bao, R. Sanaei, J. Teng, K. P. Loh, F. J. Garcia-Vidal, C.-W. Qiu // *Phys. Rev. B.* – 2013. – V. 88. – P. 205405.
- 74 Khokhlov, N. E. Photonic crystals with plasmonic patterns: novel type of the heterostructures for enhanced magneto-optical activity / N. E. Khokhlov, A. R. Prokopov, A. N. Shaposhnikov, V. N. Berzhansky, M. A. Kozhaev, S. N. Andreev, A. P. Ravishankar, V. G. Achanta, D. A. Bykov,

- A. K.Zvezdin, V. I.Belotelov // J. Phys. D: Appl. Phys. – 2015.V. 48.– P. 095001.
- 75 Kaliteevski, M.Hybrid states of Tamm plasmons and excitonpolaritons/ M.Kaliteevski, S.Brand, R. A.Abram, I.Iorsh, A. V.Kavokin, I. A.Shelykh // Appl. Phys. Lett. – 2009.– V.95. –P. 251108
- 76 Brückner, R.Parabolic polarization splitting of Tamm states in a metal-organic microcavity/ R.Brückner, M.Sudzius, S. I.Hintschich, H.Fröb, V. G.Lyssenko, M. A.Kaliteevski, I.Iorsh, R. A.Abram, A. V.Kavokin, K.Leo // Appl. Phys. Lett. – 2012. – V.100. –P. 062101.
- 77 Afinogenov, B. I.Observation of hybrid state of Tamm and surface plasmon-polaritons in one-dimensional photonic crystals / B. I. Afinogenov, V. O.Bessonov, A. A.Nikulin, A. A. Fedyanin //Appl. Phys. Lett. – 2013. –V. 103. – P. 061112.
- 78 Kaliteevski, M.A.Reduced absorption of light by metallic intra-cavity contacts: Tamm plasmon based laser mode engineering /M. A. Kaliteevski, A. A.Lazarenko// Tech. Phys. Lett. –2013. –V. 39.– P. 698–701.
- 79 Rahman, SK. S.-U.Observation of a hybrid state of Tamm plasmons and microcavityexcitonpolaritons / SK. S.-U. Rahman, T. Klein, S. Klemmt, J. Gutowski, D. Hommel, K. Sebald // Sci. Rep. – 2016. –V. 6. –P. 34392.
- 80 Liu, H. Large electromagnetic field enhancement achieved through coupling localized surface plasmons to hybrid Tamm plasmons / H. Liu, J. Gao, Z. Liu, X. Wang, H. Yang, H. Chen // J. Opt. Soc. Am. B.– 2015. – V. 32. – P. 2061–2067.
- 81 Gessler, J.Electro optical tuning of Tamm-plasmonexciton-polaritons/ J. Gessler, V.Baumann, M.Emmerling, M.Amthor, K.Winkler, S.Höfling, C. Schneider, M. Kamp //Appl. Phys. Lett. – 2014.– V. 105 –P. 181107.
- 82 Savelev, R. S., Optical Tamm states in arrays of all-dielectric nanoparticles / R. S.Savelev, A. E.Miroshnichenko, A. A.Sukhorukov, Y. S.Kivshar //JETP Letters. –2014. –V. 100.– P. 430–433.

- 83 Treshin, I. V. Optical Tamm state and extraordinary light transmission through a nanoaperture / I. V. Treshin, V. V. Klimov, P. N. Melentiev, V. I. Balykin // *Phys. Rev. A.* – 2013. V. 88. – P. 023832.
- 84 Vetrov, S. Ya. Surface modes in “photonic cholesteric liquid crystal–phase plate–metal” structure / S. Ya. Vetrov, M. V. Pyatnov, I. V. Timofeev // *Opt. Lett.* – 2014. – V. 39. – P. 2743–2746.
- 85 Vetrov, S. Ya. Spectral and polarization properties of a ‘cholesteric liquid crystal—phase plate—metal’ structure / S. Ya. Vetrov, M. V. Pyatnov, I. V. Timofeev // *Journal of Optics.* – 2016. – V. 18. – P. 015103.
- 86 Pyatnov, M. V. Localised optical states in a structure formed by two oppositely handed cholesteric liquid crystal layers and a metal / M. V. Pyatnov, S. Ya. Vetrov, I. V. Timofeev // *Liquid Crystals.* – 2017. – V. 44. – P. 674–678.
- 87 Pyatnov, M. V. Localized optical states in a liquid-crystal structure adjacent to a metal / M. V. Pyatnov, S. Ya. Vetrov, I. V. Timofeev // *Optics and Spectroscopy.* – 2017. – V. 123. – P. 183–190.
- 88 Timofeev, I. V. Chiral optical Tamm states at the boundary of the medium with helical symmetry of the dielectric tensor / I. V. Timofeev, S. Ya. Vetrov // *JETP Lett.* – 2016. – V. 104. – P. 380–383.
- 89 Chiral Optical Tamm States: Temporal Coupled-Mode Theory / I. V. Timofeev, P. S. Pankin, S. Y. Vetrov, V. G. Arkhipkin, W. Lee, V. Y. Zyryanov // *Crystals.* – 2017. V. 7. – P. 113.
- 90 Dolganov, P. V. Photonic liquid crystals: Optical properties and their dependence on light polarization and temperature / P. V. Dolganov, G. S. Ksyonz, V. K. Dolganov // *Phys. Solid State.* – 2013. – V. 55 – P. 1101.
- 91 Lakhtakia, A. Dielectric thin-film helicoidal bianisotropic medium bilayers as tunable polarization-independent laser mirrors and notch filters / A. Lakhtakia, A. C. Venugopal // *Microw. Opt. Technol. Lett.* – 1998. V. 17. – P. 135–140.

- 92 Gevorgyan, A .A., Reflection and Transmission of Light by Cholesteric Liquid Crystal–Glass–Cholesteric Liquid Crystal and Cholesteric Liquid Crystal(1)–Cholesteric Crystal(2) Systems / A .A. Gevorgyan, K. V.Papoyan, O. V.Pikichyan. // Opt. and Spectr. – 2000. V. 88.P. 586–593.
- 93 Gevorgyan, A. H. Photonic band gaps from a stack of right- and left-hand chiral photonic crystal layers. / A. H.Gevorgyan// Phys Rev E. – 2012. V. 85. – P. 021704.
- 94 Mitov, M. Going beyond the reflectance limit of cholesteric liquid crystals. / M.Mitov, N.Dessaud// Nat. Mat. – 2006. – V. 5. – P.361–364.
- 95 Chigrinov V. G., Kozenkov V M, Kwok H S. Photoalignment of Liquid Crystalline Materials: Physics and Applications. Wiley Series in Display Technology. Wiley, 2008.
- 96 Takatoh, K, Hasegawa M, Kodan M. Alignment Technologies and Applications of Liquid Crystal Devices / K.Takatoh, M. Hasegawa, M.Kodan // Taylor & Francis; 2005.
- 97 Rodarte, A.L.Dye-integrated cholesteric photonic luminescent solar concentrator / A.L. Rodarte, F.Cisneros, L.S.Hirst,S. Ghosh. // LiqCryst. – 2014. – V. 41. – P. 1442–1447.
- 98 Lakhtakia, A., Spectral holes in Bragg reflection from chiral sculptured thin films: circular polarization filters / A.Lakhtakia, V. C.Venugopal, M. W.McCall // Opt. Comm. – 2000. – V. 177. – P. 57–68.
- 99 Mitov, M. Cholesteric liquid crystals with a broad light reflection band / M. Mitov // Adv. Mat. – 2012. V. 24. – P. 6260–6276.
- 100 Alaverdyan, R. B. Chiral photonic crystals with an electrically tunable anisotropic defect. Experiment and theory / R. B. Alaverdyan, K. R. Allakhverdyan, A. H. Gevorgyan, A. D.Chilingaryan, Y. S. Chilingaryan // Tech. Phys. – 2010. – V. 55. –P. 1317–1323.